

DESIGN OF AN EXTENSIBLE COLONOSCOPE

by

Timur Altınsoy

B.S., Mechanical Engineering, Boğaziçi University, 2016

Submitted to the Institute for Graduate Studies in
Science and Engineering in partial fulfillment of
the requirements for the degree of
Master of Science

Graduate Program in Mechanical Engineering

Boğaziçi University

2019

ACKNOWLEDGEMENTS

First of all, I would like to express my gratitude to my advisor Professor Samur for his guidance and support. It would not be possible to complete my thesis without the help of him. Also, I would like to thank Prof. Yılmaz and Prof. Bebek who accepted to be evaluation committee members.

I sincerely thank my friends in Haptics and Robotics lab for their support and help throughout my thesis. I am especially grateful to my friends in the RoboCol project, including Şeref Kemal Talaş for preparing every electronic hardware and control software I needed, Bora Baydere for his ideas and help on the design, Cem Tutcu for his contributions to the prototype and Taylan Atakuru for his insights on the design. I would also like to mention my thankfulness to Günay Turan for his guidance on electronic hardware. I would like to express a special thanks to my girlfriend Ece Yayla for all her love, support and patience. You have always been there for me through thick and thin.

Last but not the least, I am more than grateful to my dear family for their everlasting love and support.

This work was supported by the Scientific and Technological Research Council of Turkey (TÜBİTAK, #115E717).

ABSTRACT

DESIGN OF AN EXTENSIBLE COLONOSCOPE

Colonoscopy is the standard medical diagnosis method used to detect abnormalities in the colon. Early diagnosis of these abnormalities is crucial for colorectal cancer treatment to succeed. Even though colonoscopy is very successful at diagnosis, this hard procedure may lead to discomfort and possible complications on the colon wall. Colonoscopy requires physical effort and may take up to one hour. In this thesis, a novel colonoscope consisting of a flexible and extensible shaft and corresponding feeding mechanisms are presented. The extensible colonoscope is steered from the tip in 3-dimensional space. It navigates through the colon via growth by means of a miniaturized version of a pneumatic actuator developed in a parallel study. The shaft consists of different concentric segments built around the actuator tubings in order to supply certain amount of rigidity while still being flexible enough to bend at certain radii. At the feeding side, the feeding mechanisms work together to control and advance the tip. Unlike the conventional colonoscopy procedures, force providing forward motion to the colonoscope is applied at the tip. Thus, pressure on the colon wall is expected to be reduced eliminating any serious complications.

ÖZET

UZAYABİLİR BİR KOLONOSKOP TASARIMI

Kolonoskopi, kolondaki polip, lezyon ve kanserli doku oluşumu gibi anomalileri tespit etmek için kullanılan standart bir tıbbi tanı yöntemidir. Bu anomalilerin erken teşhisi, kolorektal kanser tedavisinin başarılı olması için çok önemlidir. Kolonoskopi tanıda oldukça başarılı olsa da, bu zor prosedür kolon duvarında rahatsızlık ve olası komplikasyonlara yol açabilmektedir. Üstelik, kolonoskopi fiziksel çaba gerektirmekte ve bir saate kadar sürebilmektedir. Bu tez çalışmasında, esnek ve uzayabilir bir shaft ve ilintili besleme mekanizmalarından oluşan yeni bir kolonoskop tasarlanmıştır. Uzayabilir kolonoskop üç boyutlu uzayda uçtan sürülmektedir. Paralel bir çalışmada geliştirilen pnömatik bir eyleyicinin hedef kolonoskop boyutlarındaki bir versiyonu sayesinde, kolon boyunca büyüme yoluyla ilerler. Tasarlanan shaft, belirli yarıçaplarda bükülecek kadar esnek olmakla birlikte, belirli miktarda sertlik sağlamak için eyleyici borularının etrafına inşa edilmiş farklı eş merkezli katmanlardan oluşur. Besleme tarafında, ayrı besleme mekanizmaları ucu kontrol etmek ve ilerletmek için birlikte çalışır. Geleneksel kolonoskopi işlemlerindekinin aksine, ileri yönde hareketi veren kuvvet arkadan itme yerine uçtan çekme ile uygulanmaktadır. Buna bağlı olarak, kolon duvarı üzerindeki baskının azaltılması ve dolayısıyla ciddi komplikasyonların giderilmesi beklenmektedir.

TABLE OF CONTENTS

ACKNOWLEDGEMENTS	iii
ABSTRACT	iv
ÖZET	v
LIST OF FIGURES	viii
LIST OF TABLES	xiv
LIST OF SYMBOLS	xv
LIST OF ACRONYMS/ABBREVIATIONS	xvii
1. INTRODUCTION	1
1.1. Medical Background	1
1.1.1. Colonoscopy Procedure	1
1.1.2. Anatomy of the Colon	3
1.2. Motivation	4
1.3. Objectives	5
2. LITERATURE REVIEW	6
2.1. Enhancements on Conventional Colonoscopy	6
2.2. Colon Capsule Endoscopy	8
2.3. Robotic Colonoscopy	9
3. MATERIALS AND METHODS	17
3.1. Overview of the Actuator	17
3.2. Design Requirements	20
3.3. In-Vivo Section Design	20
3.3.1. Miniaturized 3-DOF PRD	21
3.3.2. Design of the Body	23
3.3.2.1. Sheath	23
3.3.2.2. Shell	26
3.3.2.3. Shaft	27
3.4. In-Vitro Section Design	27
3.4.1. Feed Mechanisms	29

3.4.1.1.	Tubing Feed	29
3.4.1.2.	Shell Feed	31
3.4.1.3.	Sheath Feed	36
3.4.2.	Pneumatic System	38
3.4.3.	Control System	39
4.	RESULTS AND DISCUSSION	41
4.1.	Actuator Performance	41
4.2.	Stiffness and Bending Capabilities	43
4.3.	Navigation Capability	44
5.	CONCLUSION	48
5.1.	Contributions and Originality	48
5.2.	Outlook and Future Work	49
	REFERENCES	50
	APPENDIX A: DATASHEETS	61
	APPENDIX B: TECHNICAL DRAWINGS	67

LIST OF FIGURES

Figure 1.1.	(a) Visual representation of a colonoscope in the colon, (b) tip of the colonoscope, and (c) camera view of the colon. Reprinted from [5].	1
Figure 1.2.	The distal end and the control knob of a colonoscope. Reprinted from [12].	2
Figure 1.3.	Sections of the large intestine. Reprinted from [19].	4
Figure 2.1.	Shape-locking guide. The atraumatic tip and the handle used to change the stiffness configuration could be seen. Reprinted from [28].	6
Figure 2.2.	Transparent cap and the cap attached to the tip of a colonoscope. Reprinted from [36].	7
Figure 2.3.	Third-Eye Retroscope (A), and colon image from it (B,C). Reprinted from [38].	8
Figure 2.4.	Third-eye panoramic device. Reprinted from [39].	8
Figure 2.5.	Colon Capsule Endoscopy (CCE). Reprinted from [42].	9
Figure 2.6.	Flex Robotic System of Medrobotics. Reprinted from [58].	11
Figure 2.7.	(a) The flexible probe of the Endotics system. (b) The locomotion principle of the Endotics system. Reprinted from [63].	12
Figure 2.8.	Independently actuated segments of the NeoGuide Endoscopic System through its colonoscope shaft. Reprinted from [66].	13

Figure 2.9.	Aer-O-Scope colonoscope system. Workstation (A), disposable colonoscope shaft (B) and distal tip (C). Reprinted from [68].	13
Figure 2.10.	ColonoSight system. Control hub, colonoscope shaft and the sleeve can be seen. Reprinted from [70].	14
Figure 2.11.	Invendoscope SC40 shaft (A) and the control driving unit (B). Reprinted from [71].	15
Figure 3.1.	The overall system. <i>In-vitro</i> and <i>in-vivo</i> sections can be seen. . . .	17
Figure 3.2.	A one degree of freedom pinch-roller mechanism allowing force exertion only at the axial direction. Reprinted from [74].	18
Figure 3.3.	A one degree of freedom pinch-roller mechanism allowing force exertion only at the axial direction. Reprinted from [76].	19
Figure 3.4.	Miniaturized 3-DOF actuator consisting of 3 PRDs.	21
Figure 3.5.	Manufactured parts of the miniaturized 3-DOF pinch-roller drive.	22
Figure 3.6.	Assembly of the 3-DOF pinch-roller drive. Scale in photos is in cm.	23
Figure 3.7.	Concentric design of the colonoscope body.	24
Figure 3.8.	The colonoscope body. Shell, sheath and slack tubings can be seen with 3-DOF PRD at the tip. Sheath is in compressed state for presentation purposes.	24
Figure 3.9.	Extension of the sheath: (a) Fully extended, (b) unloaded form and (c) fully compressed.	25

Figure 3.10.	Dimensions of the helix shell in mm. Scale at the bottom is in cm.	26
Figure 3.11.	Diagram of the concentric system along with the successive <i>in-vitro</i> feed mechanisms.	28
Figure 3.12.	Overall picture of the feed mechanisms and pneumatic system. . .	28
Figure 3.13.	Actuation mechanism of the tubing feed.	30
Figure 3.14.	A picture of the manufactured tubing feed mechanism.	31
Figure 3.15.	Planetary gear train of the shell feed mechanism. Each gear is shown and described and tooth numbers are given. Note that module of every gear is 2.	33
Figure 3.16.	Planetary gear diagram describing aforementioned speeds.	34
Figure 3.17.	Prototype of the final shell feed mechanism and the design of the planetary gear train. Stepper motors and spool are also shown. . .	35
Figure 3.18.	An image of the sheath reservoir and feed. Flexible sheath is released when its diameter is reduced to a certain value via axial force.	37
Figure 3.19.	Assembly of the pneumatic system.	38
Figure 3.20.	Schematic of the control system.	39
Figure 3.21.	Graphical user interface of the system.	40
Figure 4.1.	Miniaturized 3-DOF PRD with 2 meter long double layered tubings.	41

Figure 4.2.	Thickness of the manufactured double layered tubings. Wall thickness corresponds to half of the value read (165 μm) since two layers of wall is measured.	42
Figure 4.3.	The body at a certain tubing configuration with non-inflated 2 meter long double layered tubings when the shell is stiffened (a), and the body when the shell is in free state (b).	43
Figure 4.4.	180° bending of the body actuated in a tendon-driven fashion via slack tubings at the end of a rigid tube. Three different orientations in 3D space can be seen.	44
Figure 4.5.	Manually applied axial force using a tendon connected through the center-line of the 3-DOF PRD.	45
Figure 4.6.	(a) Minimum/maximum outer diameters of the sheath after feeding, and release diameter of the reservoir. Dimensions are in mm. (b) A picture of the prototype at the same configuration.	46
Figure 4.7.	Advancement of the colonoscope in an enclosed tube.	47
Figure A.1.	BLDC motor datasheet. Model with the number 539482 was used.	61
Figure A.2.	Framo Morat worm gear set datasheet. Model with the number A25U40 was used.	62
Figure A.3.	Reference drawing of ball bearings used in 3-DOF PRD.	63
Figure A.4.	Functional block diagram of A4988 stepper motor driver.	64
Figure A.5.	Features of ESCON Module 24/2 BLDCM driver board.	65

Figure A.6.	Maxon BLDCM encoder datasheet.	66
Figure B.1.	Technical drawing of shell's helical structure. All dimensions are in mm.	67
Figure B.2.	Technical drawing of 3-DOF PRD's rollers. D is 2.20 mm and 1.40 mm for outer and inner rollers respectively. All dimensions are in mm.	67
Figure B.3.	Technical drawing of 3-DOF PRD's main base. All dimensions are in mm.	68
Figure B.4.	Technical drawing of 3-DOF PRD's moving base. All dimensions are in mm.	69
Figure B.5.	Technical drawings of 3-DOF PRD's roller adjustment plate (left) and bearing cover (right). All dimensions are in mm.	70
Figure B.6.	Technical drawings of sheath retainer (top) and shell retainer (bottom) at tip. All dimensions are in mm.	71
Figure B.7.	Technical drawing showing 3-DOF PRD's assembly.	72
Figure B.8.	Technical drawing of sheath feed mechanism. All dimensions are in mm.	73
Figure B.9.	Technical drawings of worm shaft (top) and worm gear shafts (middle and bottom) used in tubing feed mechanism. All dimensions are in mm.	74

Figure B.10. Technical drawings of base sheets of tubing feed mechanism. Thickness is 5 mm. All dimensions are in mm. 75

Figure B.11. Technical drawings showing worm gear (top) and worm (middle) sub-assemblies and overall (bottom) assembly of tubing feed mechanism. 76

LIST OF TABLES

Table 2.1.	Comparison of robotic colonoscopy systems [63, 66, 67, 69–72]. . . .	16
------------	--	----

LIST OF SYMBOLS

a	Distance Between Tubing Centers
F_f	Friction Force Acting on Tubing
F_{P_x}	Pressure Force in x Direction
F_t	Tension Force on Tubing
F_x	Force in x Direction
F_y	Force in y Direction
i	Reduction Ratio
N	Number of Tooth
l_1	Length of Tubing 1
l_2	Length of Tubing 2
l_3	Length of Tubing 3
l_b	Length of Backbone
p_{shell}	Pitch of Shell's Helix Structure
P	Pressure Inside Tubing
r	Radius of Tubing Roller
r_p	Radius of Planet Gear
r_r	Radius of Ring Gear
r_s	Radius of Sun Gear
r_{spool}	Radius of Tubing Spool
r_T	Outer Radius of Tubing
R	Radius of Tubing
t	Wall Thickness of Tubing
v_1	Speed of Tubing 1
v_2	Speed of Tubing 2
v_3	Speed of Tubing 3
v_A	Speed of Point A
v_b	Speed of Backbone
v_B	Speed of Point B

v_C	Speed of Point C
v_{shell}	Axial Speed of Shell
v_{t_i}	Speed of i^{th} Tubing on Axial Direction
θ	Angle Between z' -axis and Diagonal Line of the Backbone
κ_b	Backbone Curvature
κ	Angle Between Roller Center And Tubing Curvature Center
μ	Friction Coefficient
ϕ	Rotation Angle of Backbone With Respect to y-axis
ω_c	Angular Speed of Carrier
ω_p	Angular Speed of Planet Gear
ω_r	Angular Speed of Ring Gear
ω_s	Angular Speed of Sun Gear
ω_{s_1}	Angular Speed of Shell Input 1 Motor
ω_{s_2}	Angular Speed of Shell Input 2 Motor
ω_{t_1}	Angular Speed of Tubing 1 Spool
ω_{t_2}	Angular Speed of Tubing 2 Spool
ω_{t_3}	Angular Speed of Tubing 3 Spool
ω_{t_i}	Angular Speed of i^{th} Tubing Spool

LIST OF ACRONYMS/ABBREVIATIONS

3D	Three Dimensional
ABS	Acrylonitrile Butadiene Styrene
BLDC	Brushless Direct Current
BLDCM	Brushless Direct Current Motor
CAD	Computer Aided Design
CCE	Colon Capsule Endoscopy
CCE-2	Second Generation Colon Capsule Endoscopy
CI	Cecal Intubation
CNC	Computer Numerical Control
cRIO	CompactRIO Real-Time Controller
CRC	Colorectal Cancer
DC	Direct Current
DOF	Degree of Freedom
GUI	Graphical User Interface
MIS	Minimally Invasive Surgery
NES	NeoGuide Endoscopic System
NPN	Negative-positive-negative
OD	Outer Diameter
PA	Polyamide
PE	Polyester
PGS	Planetary Gear System
POM	Polyoxymethylene
PRD	Pinch-Roller Drive
PS	Pneumatic System
PT	Pressure Transmitter
PTFE	Polytetrafluoroethylene
PWM	Pulse-Width Modulation
SFM	Shell Feed Mechanism

SG-1	Shape-Locking Guide
SPDC	Self-Propelled Disposable Colonoscope
TFM	Tubing Feed Mechanism
TORS	Transoral Robotic Surgery

1. INTRODUCTION

Cancer is one of the most widespread reasons of deaths in the world, and colorectal cancer (CRC) is the fourth most lethal type [1]. In 2012, 694,000 cases of CRC concluded with death where a total of 1.4 million cases were diagnosed [2]. CRC is curable if it is diagnosed at early stages [3]. The diagnosis of CRC is possible by screening of the colon. Currently the most effective screening method is colonoscopy [4].

1.1. Medical Background

1.1.1. Colonoscopy Procedure

Since the development of endoscopic devices, the importance of endoscopic applications is increasing because they provide faster and better diagnosis of abnormalities in certain sections of the body. Colonoscopy is an endoscopic procedure used to diagnose any abnormalities visually in the colon, and it is one of the most commonly used endoscopy applications and diagnosis method for colorectal cancer.

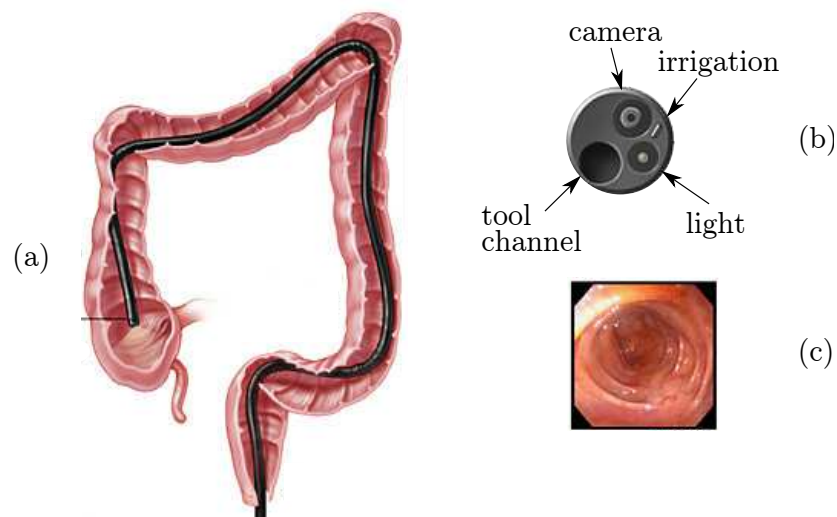


Figure 1.1. (a) Visual representation of a colonoscope in the colon, (b) tip of the colonoscope, and (c) camera view of the colon. Reprinted from [5].

The procedure is performed via visual examination of the colon using a colonoscope containing a camera at the tip. The first colonoscope developed dates back to 1970s [6]. The camera is mounted on the tip of a flexible endoscope which contains gas channels and cables necessary to transmit data from the camera. The intestine is inflated using these channels in order to increase the visibility and also make the endoscope navigate easier through the colon [7]. The endoscope shaft is navigated through the colon via a cable driven system. This system is controlled by a handle to make the tip bend at a certain maximum curvature in 3-axis and adjust the stiffness of the shaft [8]. Cancerous tissues or polyps can be removed by the colonoscope via suction [9]. Generally, the procedure takes around 30 minutes but when faced with complications it might take up to 1 hour [10]. Even though colonoscopes have been improved over years, colonoscopy is still a challenging process [11].

In order to perform colonoscopy successfully, the tip of the colonoscope shaft should reach the cecum and provide visual data [13] (see Figure 1.1). The total length of the large intestine is found to be 167 cm with a standard deviation of 21 cm according to studies [14]. Also, some therapeutic interventions are performed if needed during



Figure 1.2. The distal end and the control knob of a colonoscope. Reprinted from [12].

the operation. Thereby, a tool channel is included for needed tools. Water and CO₂ or air channels are also present through the colonoscope for insufflation of colon [15, 16]. These channels are connected to a control knob which also has different parts for air, water, suction and deflection controls. Last 10 cm of the flexible shaft is called the distal end and it is the only deflected part for navigation. Also deflection of the tip at high angles provides better visual feedback. The knob and the distal end can be observed in Figure 1.2.

1.1.2. Anatomy of the Colon

Anatomy of the colon may pose challenges for the colonoscopy procedure. To better understand the difficulties faced during the colonoscopy procedure, anatomy of the colon should be better understood.

The large intestine draws salts and water from nutrition wastes before they are disposed as solid from the anus. It is composed of the cecum, appendix, colon, rectum and anal canal (see Figure 1.3) [17]. The colon approximately has a length of 170 cm, and is composed of four sections [14, 17]. The ascending colon lies at the right lower quadrant of the colon for approximately 15 cm and, is connected to the small intestine via the cecum. The transverse colon passes from the top right to top left horizontally connecting the ascending colon to the descending colon. The descending colon lies at the left side of the abdomen from the upper left quadrant to lower left quadrant for approximately 30 cm. Then, the last section, the sigmoid colon, starts where the descending colon ends and becomes continuous with the rectum at the end drawing an “S” shape. The sigmoid colon is poorly connected to the abdominal organs like the transverse colon while the ascending and descending colons are strictly connected [17]. This behavior of the transverse and sigmoid colons makes colonoscopy operation even more challenging. According to Avgerinos *et al.* [18], the sigmoid colon is the section where most complications, especially perforation, happen due to its curved structure and lack of connection to the abdominal organs.

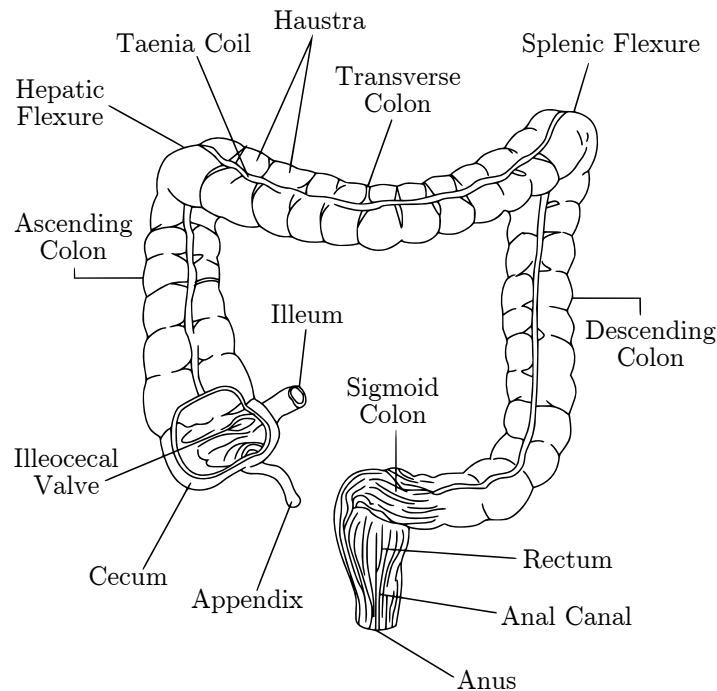


Figure 1.3. Sections of the large intestine. Reprinted from [19].

1.2. Motivation

Although colonoscopy is frequently applied, patient discomfort and some complications may occur during or after the operation. These complications are haemorrhage, post polypectomy electrocoagulation syndrome, infection, gas explosion and perforation [20–22]. Most commonly, abdominal pain and discomfort are experienced by patients after the operation [21]. Perforation happens when the bowel is forced too much and thus the internal tissue of the intestine is damaged. It is considered to be the most lethal complication [23]. It generally happens in the sigmoid colon due to its anatomy as mentioned before. According to the literature, perforation happens at a rate between 0.1% and 0.3% of the colonoscopy operations [21,23–26]. A total of 0.3% of the colonoscopy operations end up with death during or after the operation [21]. Although this rate is small, it adds up to a large number of incidence when the total number of the colonoscopies performed annually is taken to consideration. In 2012, 15 million colonoscopy operations were reported only in the US [27]. Increasing patient comfort by eliminating these complications is the main motivation of this study.

1.3. Objectives

The purpose of this study is to design an extensible colonoscope to overcome the problems caused by the conventional colonoscopes. By pulling the colonoscope from the tip rather than forcing from the rear as in the conventional colonoscopy, post-operation complications, patient discomfort and post-procedure trauma are to be decreased while performance of the operator is increased. Aims of this study are as follows

Aim 1: To design a colonoscope body that is flexible and extensible so that it can navigate through the colon. Also it should supply some rigidity to system for pneumatic actuators to work properly.

Aim 2: To design feeding/retraction mechanisms to control extension of the colonoscope. These mechanisms will form a base that the body will grow from. The base will include an air control unit to regulate pressure within the actuators.

2. LITERATURE REVIEW

2.1. Enhancements on Conventional Colonoscopy

Colonoscopy procedure is challenging and many complications are faced during the procedure. To overcome these complications, some enhancements are made through years on the conventional colonoscopes.

Looping is a major problem in colonoscopy operation since it makes the tip of the device unable to advance further [29]. It generally happens at the sigmoid colon due to its shape, and it is a major reason for difficult operation [30]. There have been some efforts to make looping less frequent and to overcome incidents. Rigid overtubes were used as a solution for a period of time but since they caused increasing pain and can lead to higher risks of perforation, the method is not used anymore [29, 31]. A more recent approach was a shape-locking guide (SG-1) [28]. It features an outer sheath (see Figure 2.1) which can change its stiffness on demand, applied to conventional colonoscopes. However, SG-1 can only prevent looping in the sigmoid colon, and its larger diameter causes more patient discomfort and pain [32].



Figure 2.1. Shape-locking guide. The atraumatic tip and the handle used to change the stiffness configuration could be seen. Reprinted from [28].

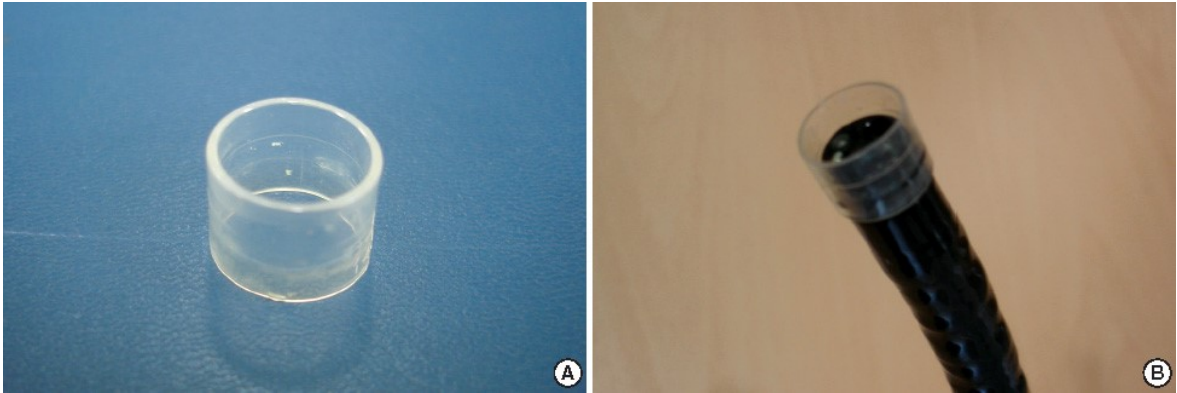


Figure 2.2. Transparent cap and the cap attached to the tip of a colonoscope.

Reprinted from [36].

In order to overcome looping, operators generally adjust stiffness of the endoscope via stiffening cables or other instruments [29]. For instance, Olympus Corporation came up with a colonoscope that its stiffness can be adjusted throughout the whole shaft with built-in tools [33]. This variable stiffness system was to cause a reduction in pain during or after the operation [34]. However, studies showed that the cecal intubation rates are lower since this colonoscope has a shorter total length [8, 35].

There were also some improvements in vision systems of colonoscopes. These include the cap-fitted colonoscopy, third eye retroscope and third eye panoramic device. The cap-fitted colonoscopy makes use of a transparent cap fitted at the tip of distal end in order to keep the camera's distance to the internal tissue of the colon; thus, providing a better visual feedback [36]. A picture of this cap can be seen in Figure 2.2. It was shown that the cap reduces the operation time significantly [37].

Third eye colonoscopy utilizes another camera which is rotated 180° from the standard one, providing a backwards view of the colon walls and a better chance to diagnose the abnormalities [38]. Third eye panoramic device is another enhancement utilizing two additional cameras at the tip, providing the better visual imagery of the colon [39]. Third eye retroscope and third eye panoramic device are very practical in the sense that they allow the operator to see behind the folds present inside the



Figure 2.3. Third-Eye Retroscope (A), and colon image from it (B,C). Reprinted from [38].

colon [40,41]. Third-Eye Retroscope and panoramic devices can be seen in Figure 2.3 and Figure 2.4, respectively.

2.2. Colon Capsule Endoscopy

Colon capsule endoscopy (CCE) is an alternative approach in which the patient swallows a capsule, and the colon is screened through an embedded camera [42]. It is especially useful in the cases where patient has small-bowel lesions or gastrointestinal bleeding [43].

However, CCE has poorer performance in polyp detection than conventional

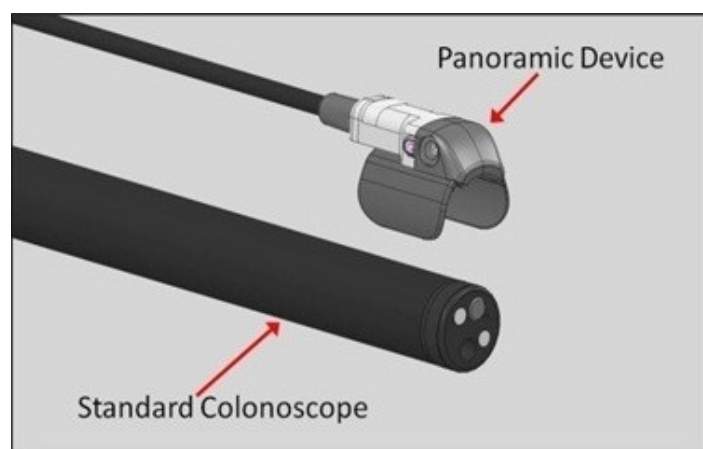


Figure 2.4. Third-eye panoramic device. Reprinted from [39].



Figure 2.5. Colon Capsule Endoscopy (CCE). Reprinted from [42].

colonoscopy [44, 45]. But it is shown in the studies that the second generation colon capsule endoscopy (CCE-2) has a relatively higher success rate compared to its previous version [46, 47]. Also bowel preparation for CCE is much more crucial than it is for conventional colonoscopy, and may lead to inadequate results since it is not possible to use water and air [47]. Colon preparation is also important for the movement of the capsule through the colon [48]. Another drawback of CCE is that, conventional colonoscopy should undergo in case of a positive result following CCE [49]. Additionally, another study showed a preference of conventional colonoscopy over CCE due to probability of repeating bowel preparation [50]. Overall, CCE could be considered as a good alternative for diagnosis since it does not require sedation or air insufflation, and is noninvasive. But it does not have any ability to treat positive results [46, 49].

2.3. Robotic Colonoscopy

Robotic applications in the medical area are getting more and more widespread. Rehabilitation robots and robotic surgery are the most common applications [51–53]. Master and slave systems are commonly used in these applications. The most well-known example of such system is the da Vinci Robot. In these systems, control algorithms are used to assist the surgeon, and minimize the errors sourcing from human imperfections. Even though this kind of robotic applications tend to be expensive,

they enhance possible surgical interventions and reduce complications faced during operation.

Minimally invasive surgery (MIS) is the operations where the necessary instrumentation is carried to the target area inside the body through a small hole alongside with a camera at the tip. Even though the performance of MIS is increased by the introduction of robotics in the medical area, it is still challenging to reach certain delicate inner parts of the human body. Open surgery is still used for medical intervention to these areas [54, 55]. Endoscopy is a procedure where inside of the body is screened using natural openings and some abnormalities are intervened if necessary [56]. In many endoscopic applications a flexible shaft is introduced to body. One of the most common endoscopic application is colonoscopy.

Continuum robots ¹ are promising solutions to compensate drawbacks of rigid-linked conventional robots in the medical use. Due to their simplicity with respect to the conventional rigid linked robots, it is possible to manufacture continuum robots in small scales. This makes continuum robots a good candidate for MIS and endoscopic operations in inner parts of the body which are hard to reach.

An example of such endoscopic robots is the Flex Robotic System of Medrobotics which is widely used in Transoral Robotic Surgery (TORS) and is a permutation of the CardioARM developed at Carnegie Mellon University (See Figure 2.6). Even though, da Vinci allows surgeons to operate in TORS, it does not provide access to certain surgical areas due to its rigid manipulators [58]. Flex Robotic System is a continuum robot composed of 50 cylindrical links connected via cables. It is a cable driven system which allows 105 degree-of-freedom with its 10-mm diameter [59]. This makes the system ideal for endoscopic surgeries since it is possible to reach more inner surgical regions. However, it is not possible to use it in colonoscopy procedures due to its relatively short length (300 mm).

¹A robot is called a continuum robot when the length of its links approaches to zero while the number of its joints approaching to infinity, i.e. infinite DOF in theory [57].

The first study for robotic colonoscopy dates back to 1995. Slatkin *et al.* [60] developed an inchworm robot locomoted like a caterpillar [61]. The locomotion concept was achieved by pads clinging to surface from the rear parts of the body, and supplying a forward extension. Clinging the front pads to surface, and retracting the body's rear part to forward enables the movement of the frontal part of the body [60]. This study has inspired the Endotics System which consist of a workstation and a probe having a flexible body, a steerable distal end, a head to accompany visual systems, water jet and air channels [60, 62]. The actuation of the distal end was achieved by pads at the proximal and distal ends clamping to mucosa of the colon in a similar way to the Inchworm robot [62, 63]. First, proximal chamber clamps on the colon wall. Then both chambers clamp on the wall and extension achieved with worm mechanism. Finally, unclamping of the proximal chamber is followed by contraction of the worm mechanism.

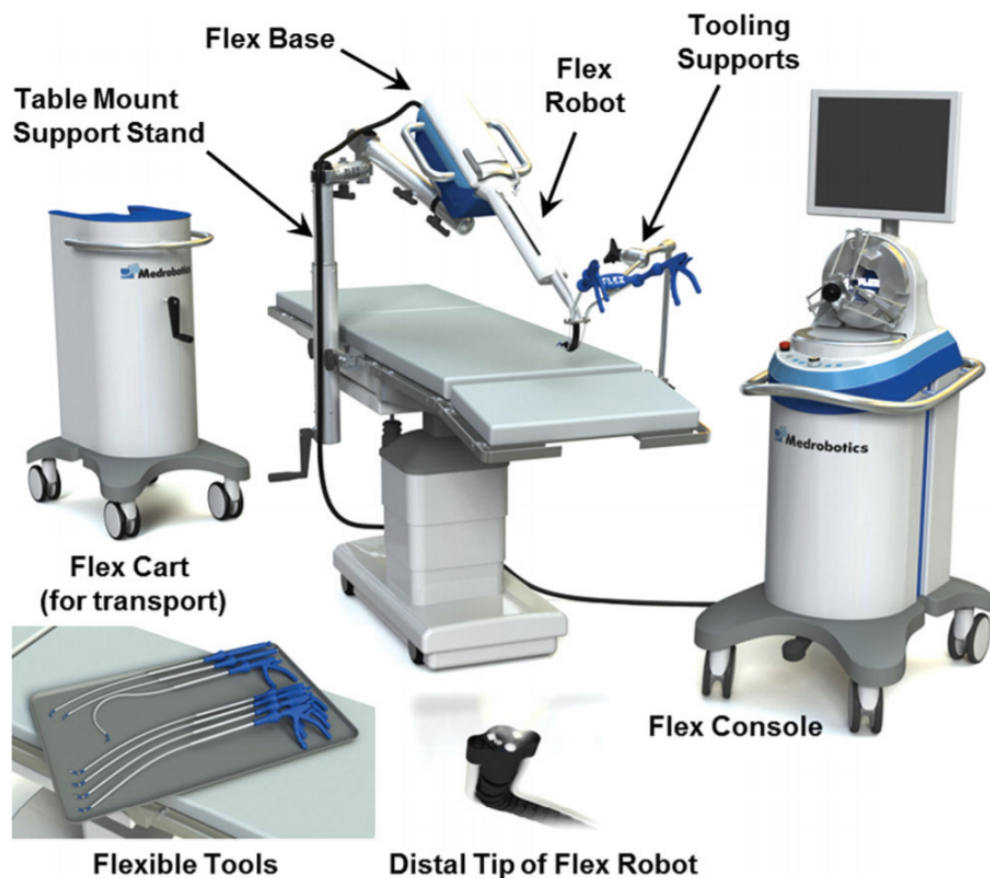


Figure 2.6. Flex Robotic System of Medrobotics. Reprinted from [58].

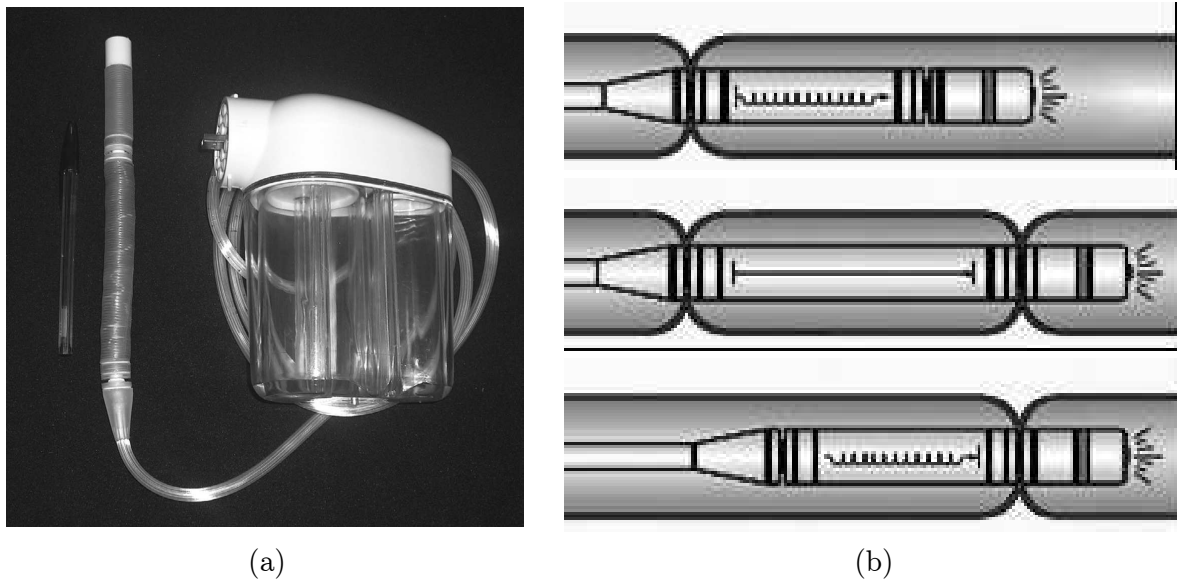


Figure 2.7. (a) The flexible probe of the Endotics system. (b) The locomotion principle of the Endotics system. Reprinted from [63].

A picture of Endotics probe and locomotion principle can be seen in Figure 2.7. In the studies, it was shown that Endotics system reduced the pressure applied to the colon wall as compared to the conventional colonoscopy [63]. Also its diagnostic abilities were shown to be similar even though it could not achieve cecal intubation (CI) in all cases [64]. It is also worth mentioning that CI mean time was approximately half of the conventional colonoscopy and was applied without narcotization [64].

Another robotic device for colonoscopy is NeoGuide Endoscopic System (NES) developed by Eickhoff *et al.* [65]. This device used different segments of same length which were actuated separately through the colonoscope shaft. This actuation supplied a snake like locomotion to the device and the colonoscope takes the shape of the colon to prevent perforation and other complications faced during the colonoscopy. The colonoscope movements are recorded using a position sensor at the tip and the shaft preserves its shape throughout the procedure. Advancement of the device is provided by the operator manually [66]. In the in-vitro tests of the device, it was seen that force applied to the colon wall and the displacement of the colon during the operation were lower compared to conventional colonoscopes [65]. First clinical studies showed that



Figure 2.8. Independently actuated segments of the NeoGuide Endoscopic System through its colonoscope shaft. Reprinted from [66].

NES was a feasible robotic device for colonoscopy operation and loop formation was significantly reduced [67].

Another approach in robotic colonoscopy is balloon assisted colonoscopy. An example of such devices is Aer-O-Scope utilizing the self-propelled disposable colonoscope (SPDC) system developed by Vucelic *et al.* [69]. Actuation of the disposable colonoscope was made by increasing the pressure at the colon area between two in-

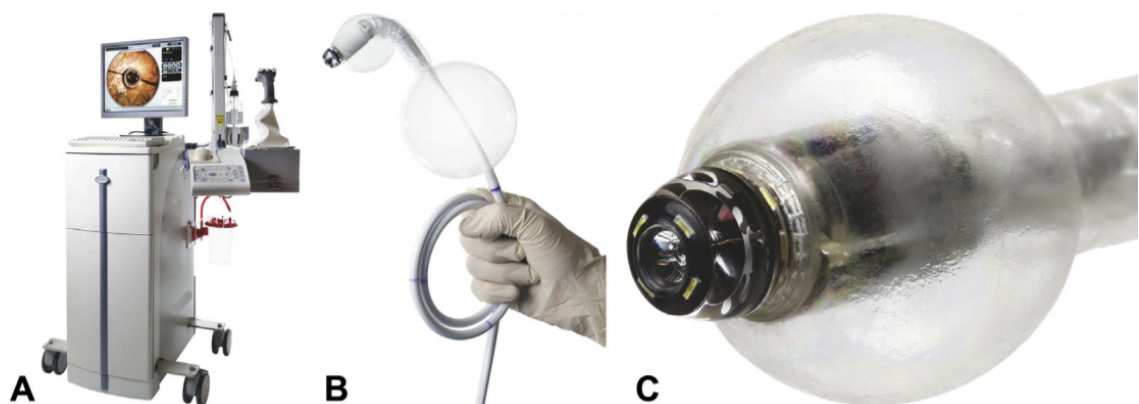


Figure 2.9. Aer-O-Scope colonoscope system. Workstation (A), disposable colonoscope shaft (B) and distal tip (C). Reprinted from [68].

flated balloons sealing the inner surface of the colon (one stationary one mobile) thus moving forward the mobile balloon, i.e. tip of the colonoscope, which slides along the colon [69].

ColonoSight is another example of robotic colonoscopy applications [70]. It consists of a disposable sleeve and a colonoscope shaft similar to conventional ones (see Figure 2.10). It works in the same manner with the conventional colonoscopes except propulsion. Advancement of the shaft is provided by the axial force generated by a sleeve by means of a pneumatic system [70]. This sleeve also protects the shaft against the corrosive environment of the colon, and makes it possible to use the shaft again. Also, forward force can be achieved by the same manner as the conventional colonoscopes; by pushing from behind. In medical trials of the device, no complications were observed during or after operation [70].

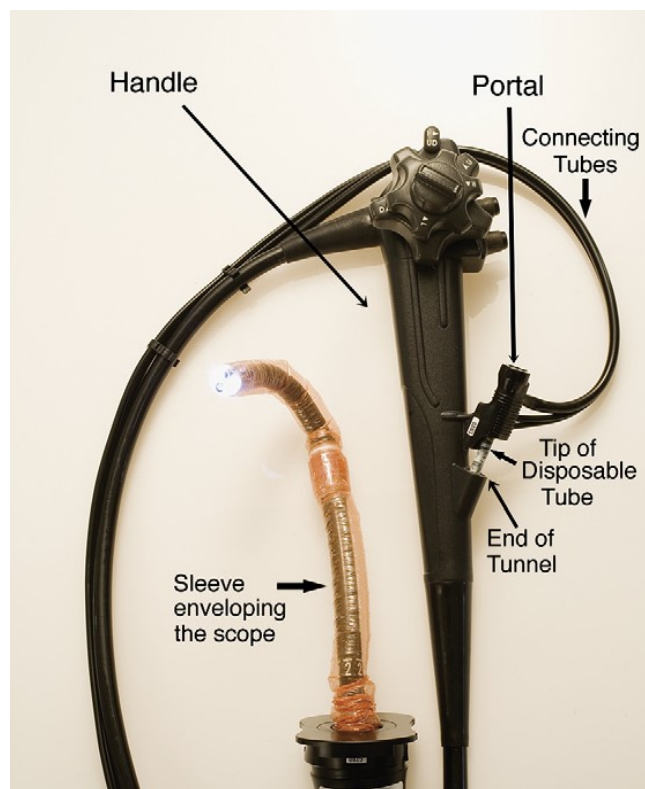


Figure 2.10. ColonoSight system. Control hub, colonoscope shaft and the sleeve can be seen. Reprinted from [70].

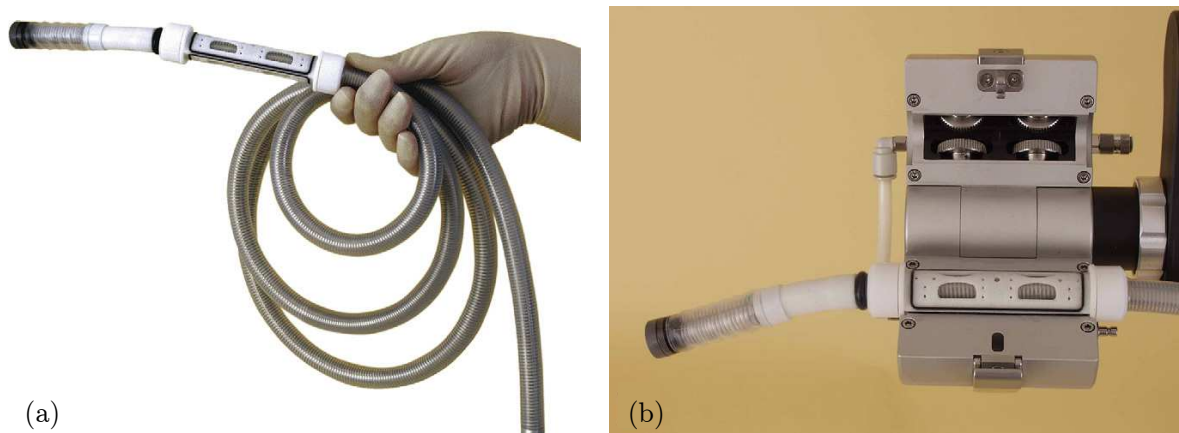


Figure 2.11. Invendoscope SC40 shaft (A) and the control driving unit (B). Reprinted from [71].

Invendoscope is a motor driven endoscope which uses growing as advancement method through the colon [71]. The force in the axial direction is applied 10 cm away from the tip, thus reducing the lateral force applied to the colon wall. It features a hand held driving unit and a disposable shaft. The shaft is in a similar fashion to the conventional colonoscopes in terms of therapeutic operations [71]. In clinical trials, a high rate of CI was achieved. In the medical trials using a second generation prototype (SC40), pain ratings were 0% [71]. A picture of SC40 prototype and its driving unit can be seen in Figure 2.11.

Overall, many of these developed robotic systems show promising characteristics. Even though CI rates are lower mostly, CI times are significantly lower compared to conventional colonoscopy. In some systems sedation was not required since pain ratings were very low due to their actuation principles. Except for Aer-O-Scope, a tool channel is present. Even though *in-vivo* experiments are limited to a small participant number, no serious complications were faced during these pilot studies. A comparison of these systems in terms of *in-vivo* performance and different capabilities is given in Table 2.1.

Table 2.1. Comparison of robotic colonoscopy systems [63, 66, 67, 69–72].

	CI Rate	CI Time	Procedure Time	Tool Channel	Sedation
Endotics	82%	n.a.	45.1 min	Yes	No
Neoguide	100%	20 min	n.a.	Yes	Yes
Aer-O-Scope	83%	14 min	26 min	No	No
Colonsight	90%	11.2 min	n.a.	Yes	Yes
Invendoscope	98%	16.4 min	32.8 min	Yes	No

3. MATERIALS AND METHODS

The proposed colonoscope is composed of two sections: *in-vivo* and *in-vitro* (see Figure 3.1). *In-vivo* section represents the colonoscope shaft itself when extended. During operation the colonoscope shaft navigates by means of growing. This means that material is added to the shaft to advance the colonoscope. This is achieved by feeding different segments concentrically from successive feeding mechanisms, which compose the *in-vitro* section.

In the following sections, first the actuation principle of the colonoscope is explained, and then the design requirements are given. Later, design of the colonoscope shaft, including the actuator, are overviewed and design details are explained in Section 3.3. In Section 3.4 feeding mechanisms, pneumatic and control systems are presented.

3.1. Overview of the Actuator

The proposed colonoscope is pneumatically actuated. The pneumatic actuators used to exert force at the tip are based on so-called pinch-roller drive (PRD) developed in a parallel study [73, 74]. Three PRDs are used to obtain three bending degrees of freedom [75]. This 3-DOF PRD is miniaturized to be used in a colonoscope shaft [76].

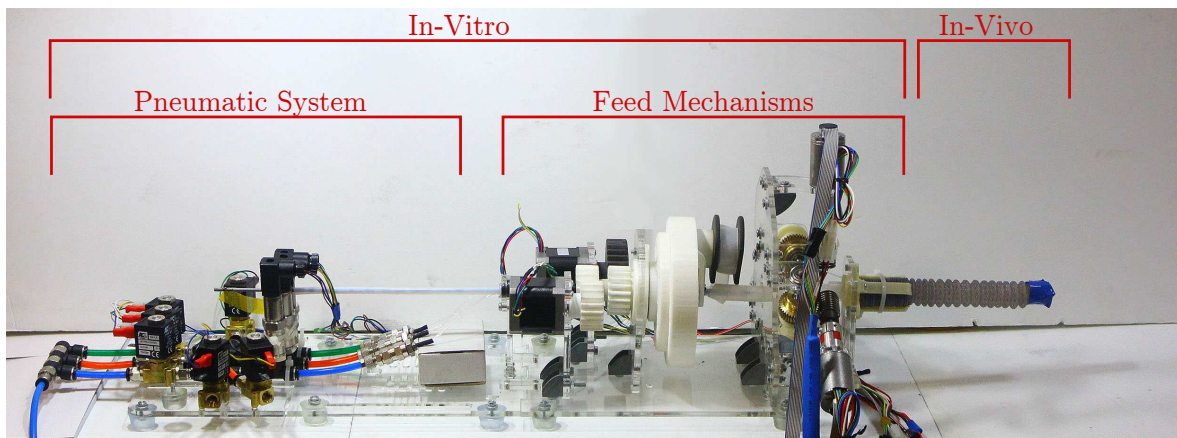


Figure 3.1. The overall system. *In-vitro* and *in-vivo* sections can be seen.

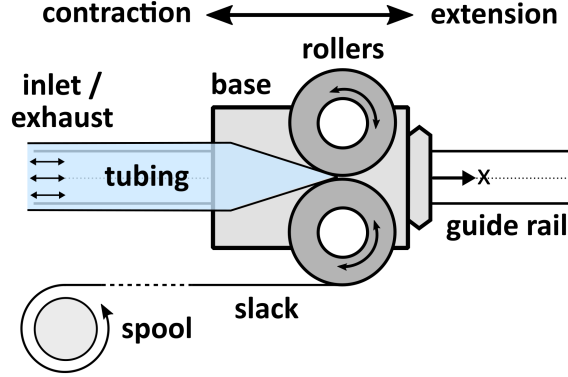


Figure 3.2. A one degree of freedom pinch-roller mechanism allowing force exertion only at the axial direction. Reprinted from [74].

The working principle of the actuator is based on conversion of potential energy of pressurized air to kinetic energy. A thin-walled inflatable tubing is squeezed in between two frictionless rollers which are anchored on a base. The air pressure at one side of the tubing exerts an axial force on the rollers. The slack section on the other side is connected to an electric motor in order to control the speed and displacement of the roller base. In other words, the inflated tubing supplies the needed axial force to advance the base when the slack section is released from a spool connected to a motor [74]. A representation of a one dimensional conceptual design of the actuator can be seen in Figure 3.2.

A linear relationship between pressure at the inlet and force output was found. Even though the experiments were done on a larger scale tubings, developed model can be used in the final scale system, i.e. 3 mm OD tubings. A free body diagram of the forces can be seen in Figure 3.3. Force equation is given by Equation 3.1 and 3.3 [74].

$$F_x = F_T (e^{\mu\kappa} - \cos(\kappa)) + F_{Px} \quad (3.1)$$

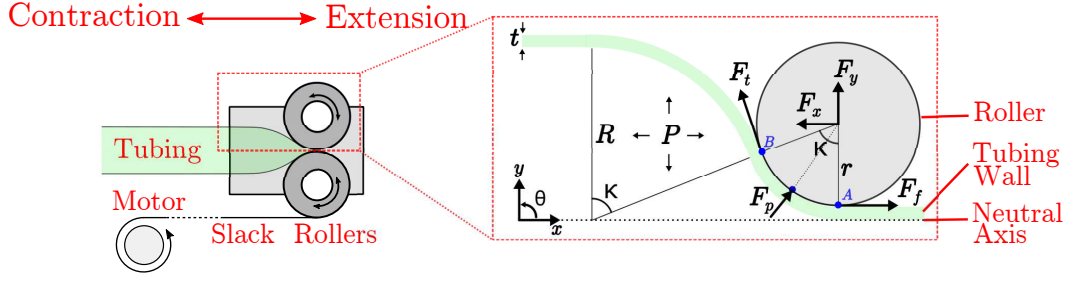


Figure 3.3. A one degree of freedom pinch-roller mechanism allowing force exertion only at the axial direction. Reprinted from [76].

F_t and F_{Px} are given in Equations 3.2 and 3.3 [74].

$$F_{Px} = \int_0^{\kappa} \sin \theta \pi \cdot (R - R_{\theta}) r_t d\theta \quad (3.2)$$

$$F_t = P\pi R^2 \quad (3.3)$$

R_{θ} , r_t and κ are given in Equations 3.4 to 3.6 [74].

$$R_{\theta} = r_t (1 - \cos \theta) \quad (3.4)$$

$$r_t = r + t \quad (3.5)$$

$$\kappa = \cos^{-1} \left(\frac{r_t}{R + r_t} \right) \quad (3.6)$$

We showed that when three pinch-roller drives are used at the tip, navigation is possible in a growing fashion [75]. Also force output was consistent with the developed model and speed control was achieved with a spool mechanism for tubings [77].

3.2. Design Requirements

Overall length of the colonoscope should be 2 m that is determined according to the mean colon length which is 167 cm in average with a standard deviation of 21 cm [14]. While moving through the colon, colonoscopes need to make sharp maneuvers due to different turns of the colon. For this reason, the colonoscopes need to make turns up to 180° . Diameters of conventional colonoscopes ranges between 12 to 15 mm [78] whereas it is increased up to 19 mm in robotic applications [64, 69, 70]. The overall diameter of the proposed colonoscope should not exceed 17 mm for easier rectal introduction.

It is observed that, tubings of the PRD tend to buckle at medium radii of curvature. This causes dramatic displacement of the body in a quick interval of time. For safe navigation, this should be prevented by the body of the colonoscope. The overall design of the body is established around this requirement. In order to ensure safe navigation the tubings, inflated sections should be reinforced from inner and outer perimeter. Thus, two different parts should be designed to prevent such rapid changes in geometry of body.

Also the slack section of the tubings should follow back the body all the way to the feed mechanism. Tubing slacks tend to follow a straight path to feeding spools since they undergo tension caused by holding force of motors and forward force applied by PRD. This disrupts the intended navigation since overall length and orientation of the backbone is directly affected. So, these slacks should be enclosed by an additional layer in a similar way inflated sections are.

3.3. In-Vivo Section Design

The *in-vivo* section corresponds to the colonoscope shaft, which includes the backbone, or body, and the actuator at the tip. The body of the shaft is designed as three concentric parts which are built around the actuator tubings to supply the

required rigidity of the backbone. In this section an overview of the actuator is given, and then the design of the colonoscope body is explained in detail.

3.3.1. Miniaturized 3-DOF PRD

A miniaturized version of the aforementioned actuator was designed in order to be used in colonoscopy. The design has a similar fashion to the one developed by Baydere *et al.* [73]. The main difference is the size of the parts. Since an outer diameter of 16 mm was aimed, material and design alterations were made. The actuator was designed with double guide shafts and only one tightening screw for each PRD for better parallel placement of rollers. The diameter of these guides are 1 mm. Ball bearings with an inner diameter of 0.5 mm and outer diameter of 1.5 mm are used in this design. Bearing covers are used to retain the ball bearings in place since a tight fit was not applicable for these bearings. Rollers have 1.40 mm and 2.20 mm diameters. M1.2 screws are used for tightening of the rollers, bearing covers and mounting of other parts on both ends. Figure 3.4 shows the final design of miniaturized 3-DOF PRD.

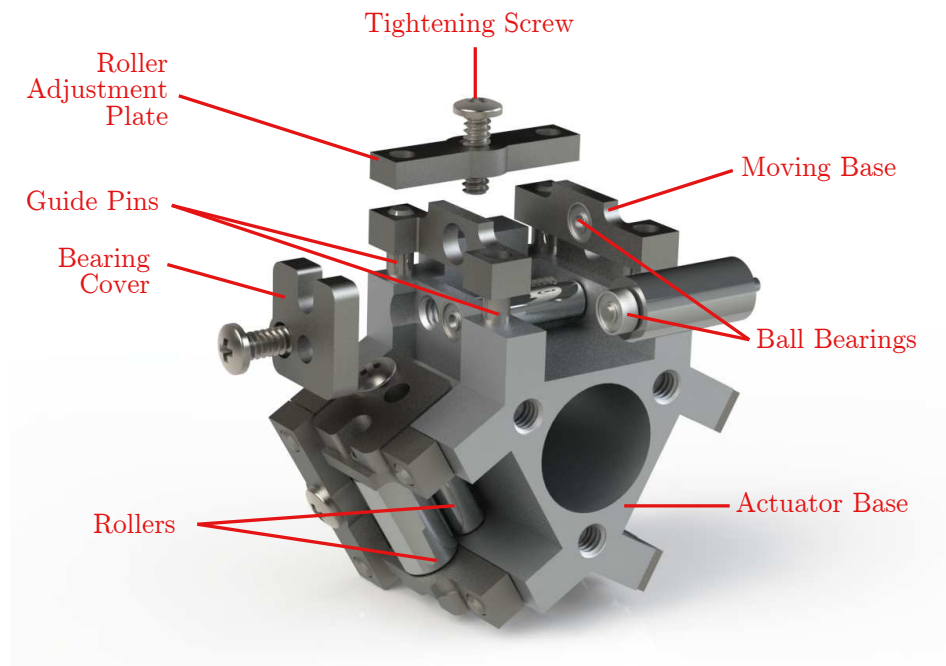


Figure 3.4. Miniaturized 3-DOF actuator consisting of 3 PRDs.

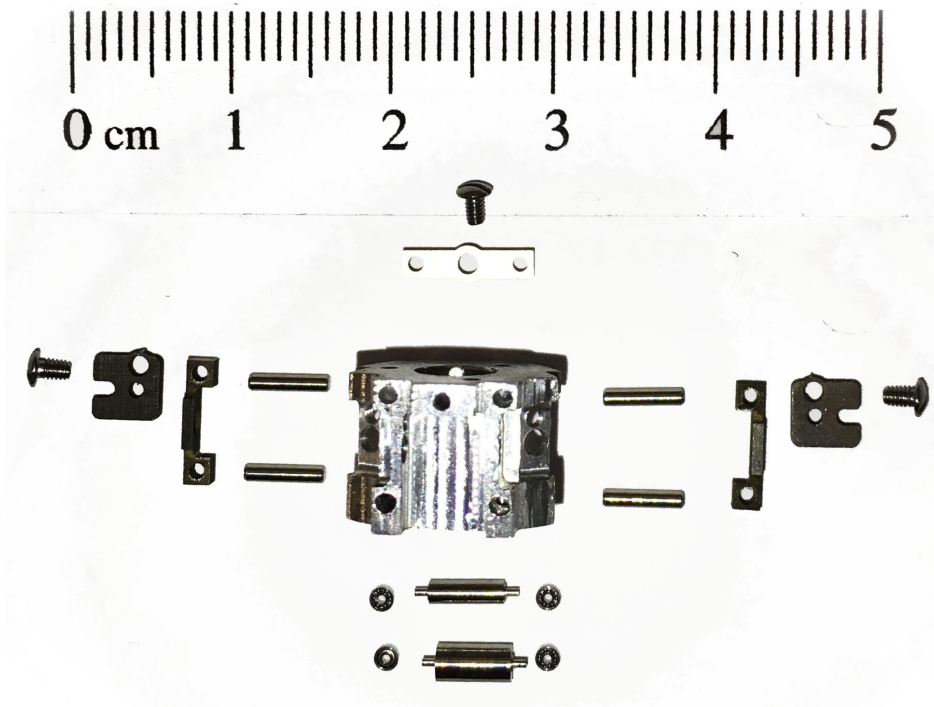


Figure 3.5. Manufactured parts of the miniaturized 3-DOF pinch-roller drive.

Base material is Aluminum 7075-T6 alloy. This alloy has low density and high tensile strength. Its yield strength is 435 MPa and density is 2.81 g/cm^3 [79]. AISI 302 stainless steel was used for the rollers due to its rigid nature and ease of machining. Roller adjustment plate, moving base and bearing covers are manufactured from AISI 304 stainless steel for the same rigidity reason and its availability as sheet metal. Both stainless steel types have a Young's Modulus of 193 GPa [80, 81]. Guide pins were cut from 1 mm diameter ejector pins which are made of 1.2343 hot-work steel. It has high Young's Modulus (207 GPa) and high hardness value (Rockwell C 56) which is beneficial for the assembly [82]. During the assembly, it is possible to scratch the surface of these pins and it is a non-desirable situation for snug-fit tolerances.

All parts were produced using different methods according to their needs. Actuator base was manufactured using a 5-axis CNC milling machine. Rollers were made in a specialized CNC lathe. Roller adjustment plate, moving base and bearing covers were produced in a wire erosion machine. The manufactured parts and the assembly of the 3-DOF PRD can be seen in Figure 3.5 and 3.6 respectively. The total force which

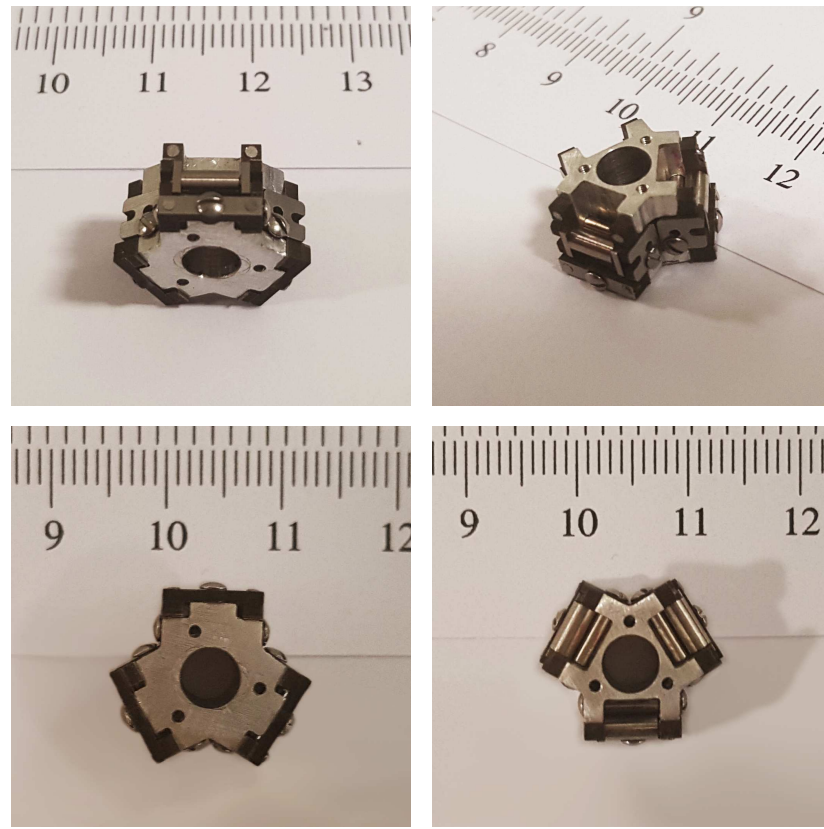


Figure 3.6. Assembly of the 3-DOF pinch-roller drive. Scale in photos is in cm.

can be obtained using this actuator with 3 mm OD tubings is estimated as 3.85 N at 300 kPa pressure using Equations 3.1 to 3.6.

3.3.2. Design of the Body

The body of the colonoscope consists of three segments: sheath, shell and shaft. These three segments are accumulated radially in order to supply rigidity for the actuator tubings while still being able to bend with minimal bending moment. Figure 3.7 shows the design of the body, and Figure 3.8 shows the assembled prototype.

3.3.2.1. Sheath. The sheath enables other parts of the main body including the shell and tubings to stay intact. Also it prevents straight elongation of the tubing slacks. It is retracted at the beginning of the *in-vitro* section with a folding mechanism when the axial force is applied.

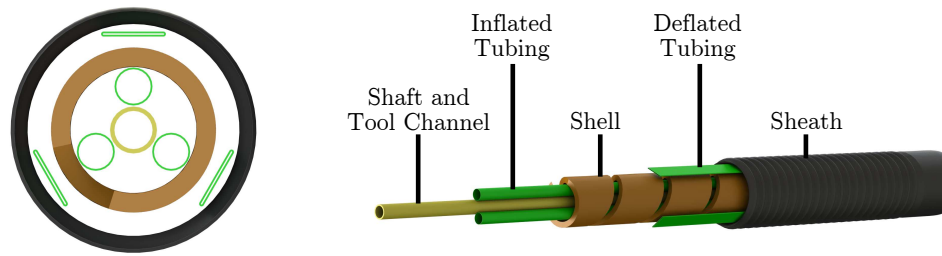


Figure 3.7. Concentric design of the colonoscope body.

The sheath is designed so that it has very low bending and axial stiffness. This ensures its easy accumulation to the corresponding reservoir. Due to its crimped nature, it can extend at very high ratios (see Figure 3.9). However, it tends to contract radially when extended with respect to its compressed state.

Off-the-shelf expandable cable sleeves were used to manufacture the sheath. Its material is polyester (PE) which is suitable for heat forming. A simple thermal forming process is applied to obtain its crimped structure. First, it is fitted on a metal pipe having a good heat conduction. Aluminum was used as pipe material. Then, it is compressed by force and anchored from both ends of the crimped structure. Finally, it is heated up to 350 °C for 5 minutes. The result of this procedure is a crimped sheath with minimal bending and axial stiffness.

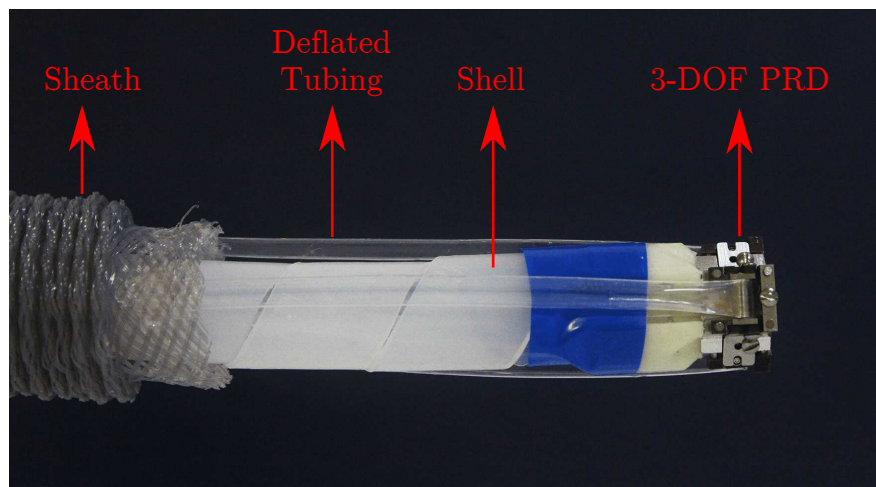


Figure 3.8. The colonoscope body. Shell, sheath and slack tubings can be seen with 3-DOF PRD at the tip. Sheath is in compressed state for presentation purposes.

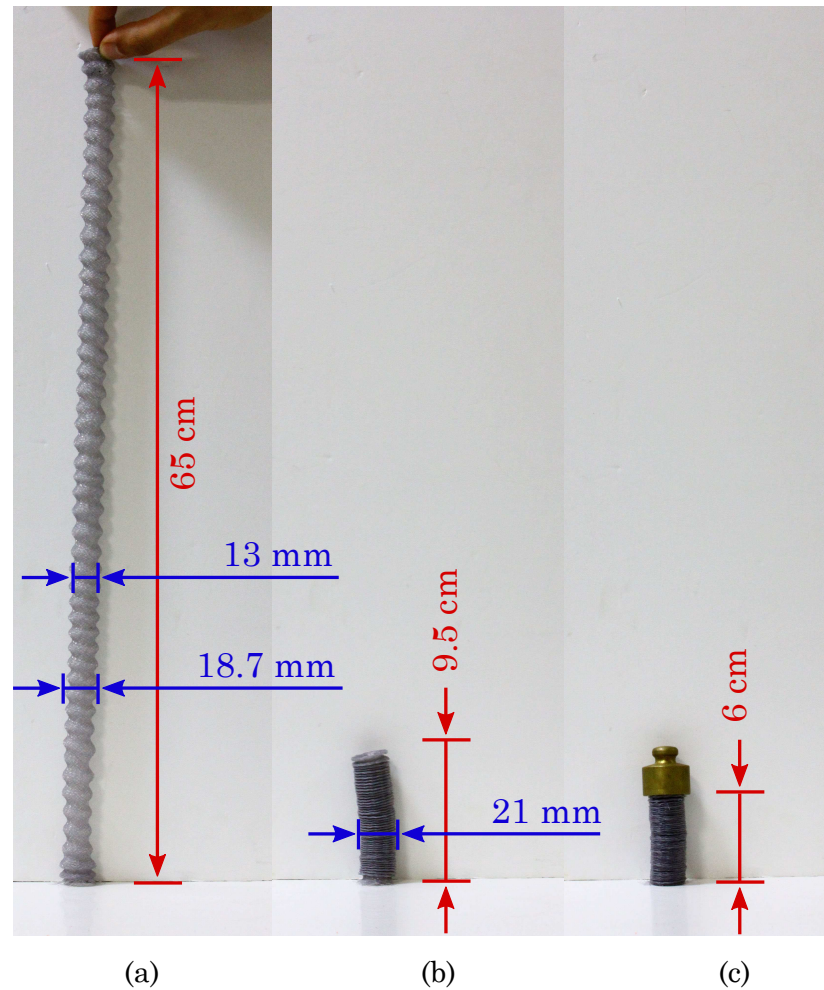


Figure 3.9. Extension of the sheath: (a) Fully extended, (b) unloaded form and (c) fully compressed.

The outer diameter of the sheath is 21 mm when its fully compressed. The extended outer diameter deviates around 13-18 mm. Since it has low radial stiffness, narrow sections of this extended form does not affect the low friction with the deflated tubings. It has an extension ratio up to 1:11 (see Figure 3.9). This allows a 20 cm compressed reservoir to be enough for up to 2 meters extended length.

Since the tubing slacks follow the sheath closely through the body, they have contact with each other on multiple places. So, the friction coefficient between the tubings and the sheath should be low ensuring minimal force losses due to friction. Polyester material of the sheath is beneficial in this sense.

The sheath is connected to the tip composed of three PRDs using a connector produced via 3D printing. The material of this connector is acrylonitrile butadiene styrene (ABS). This connector is mounted on the tip base using three M1.2 screws, and the sheath is glued to its circumference. On the other side, the sheath is anchored at a reservoir, and is passively released by its corresponding feeding mechanism.

3.3.2.2. Shell. The shell supports inflated tubings against buckling. It consists of a helix structure which go through the main body and is drawn accumulated at a roller actuated using a planetary gear system in the *in-vitro* section. Note that similar to the sheath, friction coefficient should be low between the tubings and the shell since there is a relative motion between them.

The shell consists of a uniform part which can be accumulated on a spool and be fed on top of the inflated tubings. The solution was a thin-walled plastic part with helix structure (see Figure 3.10). When accumulated on a spool pre-stressed, i.e. its natural form is helix, this shell can be released with a feeding mechanism. Helical cable wraps were a perfect off-the-shelf product for such application since they are flexible and they have the desired helical structure for feeding. The cable wrap used for this application has an outside diameter of 13 mm with a wall thickness of 1.5 mm. The

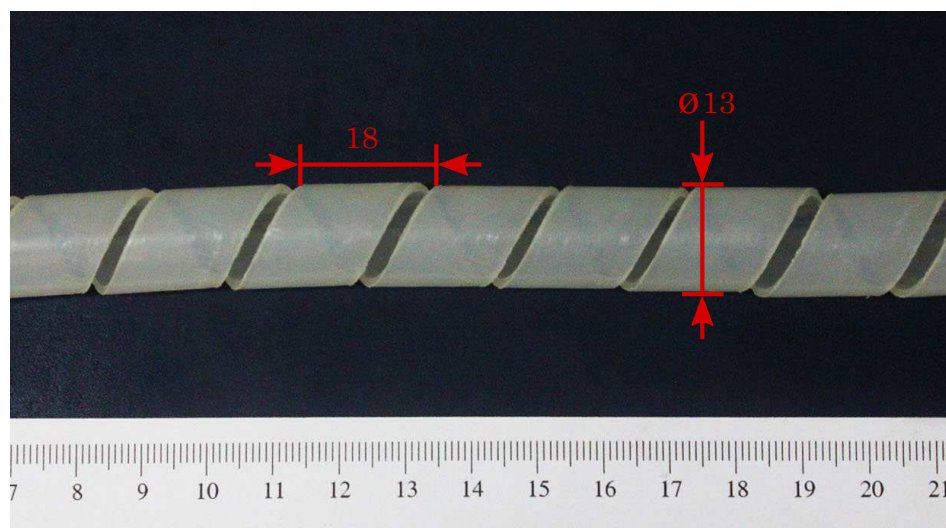


Figure 3.10. Dimensions of the helix shell in mm. Scale at the bottom is in cm.

material of the product is polyoxymethylene (POM) which is advantageous in terms of friction since POM is known to have low friction coefficients with polyamide (PA) which is outer material of the tubings.

3.3.2.3. Shaft. While the shell supports the tubings from outside, the shaft provides inner support. Necessary cabling and channels pass through the center of the shaft. It also prevents the tubings to have contact with each other so that their orientation is controlled better.

The shaft is not fed to the body like the other parts. Instead it is pulled by the force formed by the actuators at the tip. The inflated tubings grow from the tip, thus they do not have any movement in axial direction. While the tubings are stationary, the shaft advances with the same speed as the other components of the body does. Thus, a relative velocity between the shaft and the tubings forms. This implies that a low coefficient of friction should be satisfied between these two elements not to wear and tear aside from the additional losses it would cause.

Working channel of the colonoscope is also present in the center of the shaft. A 4.8 mm diameter hole at the PRD base is left for this channel to pass through. This designates shaft's outer diameter as 4.8 mm. A hollow tubing of polytetrafluoroethylene (PTFE) with 3.2 mm inner diameter is used. This material has low coefficient of friction. Also it is beneficial in terms of flexibility since PTFE's bending stiffness is not high at these dimensions.

3.4. In-Vitro Section Design

The *in-vitro* section is where the control of the body is achieved. It consists of a pneumatic system and feeding mechanisms for the tubings, shell and sheath. While the pneumatic system regulates air pressure providing forward force at the tip, the feed mechanisms control the orientation and elongation of the body. A schematic representation of the *in-vitro* section can be seen in Figure 3.11, and Figure 3.12 shows

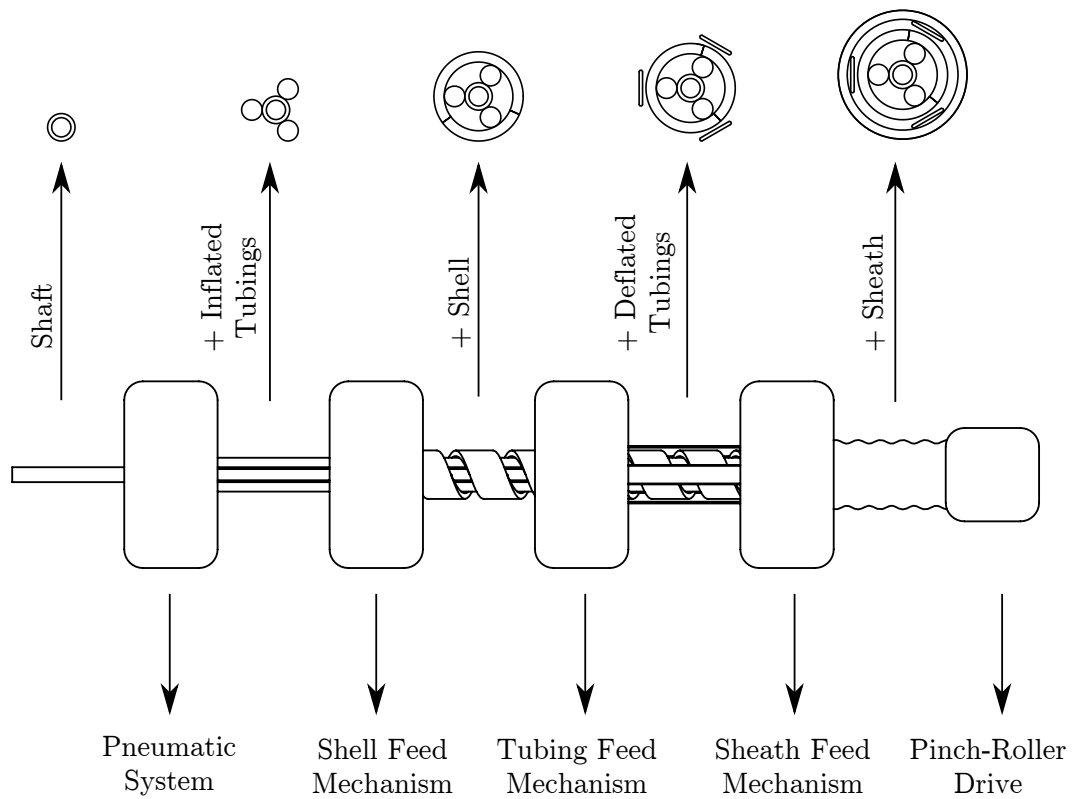


Figure 3.11. Diagram of the concentric system along with the successive *in-vitro* feed mechanisms.

the mentioned systems in the manufactured prototype. Electronic hardware and control algorithms of the feed and pneumatic systems are developed in a parallel study [77].

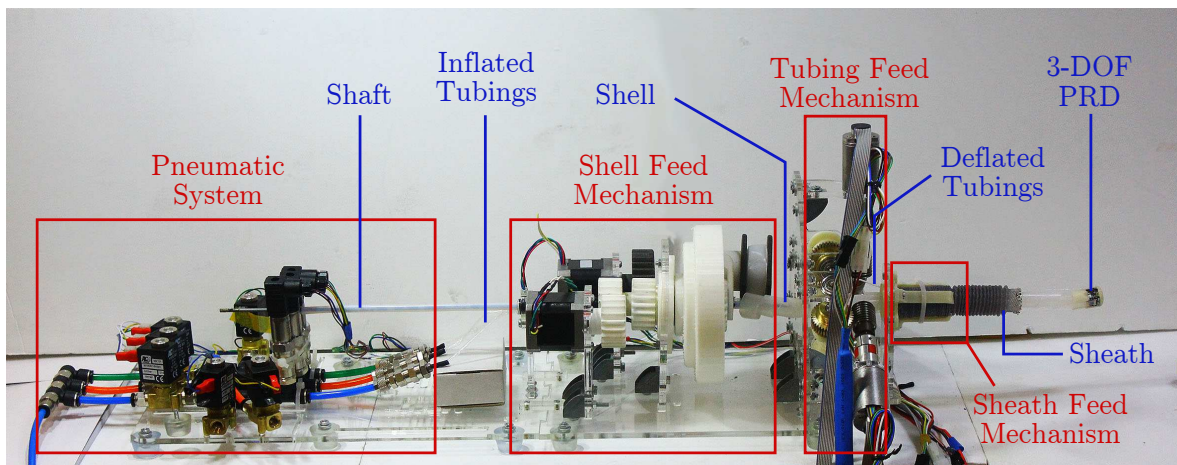


Figure 3.12. Overall picture of the feed mechanisms and pneumatic system.

3.4.1. Feed Mechanisms

In order to extend the body in a growth fashion, all parts in the colonoscope body should be accumulated and fed from the *in-vitro* section. As mentioned above; to be able to reinforce the tubings, the inflated and deflated sections should be enclosed by different parts. The deflated sections pass between the shaft and shell while the inflated sections pass between the shell and sheath. In order to ensure this structure, the feed mechanisms should work in synchrony.

The order of feeding is parallel to the order of the parts: radially from inside out. Except the shaft, all parts are accumulated on a spool in their corresponding feeding mechanism. It is drawn with the axial force formed at the tip. At the pneumatic system, the tubings are pressurized and aligned around the shaft. Note that one end of the tubings are anchored here. Then, the shell is wrapped on top of the inflated tubings with its corresponding feed mechanism. Next, the slack section of the tubings, which return from the actuator, are fed. Finally, the sheath is passively released and the assembly of the body is completed. This concept is visualized in Figure 3.11.

3.4.1.1. Tubing Feed. Feeding of the tubings is the most crucial part of the *in-vitro* section since it is directly related to navigation and speed control of the colonoscope. The deflated tubings are wrapped around their individual actuated spools. While backwards movement of the tubings is provided by these spools, forward movement is provided by the pneumatic actuator at the tip. However, the tip would propagate in an uncontrolled fashion without any restriction of the deflated tubings. Therefore, the movement is controlled via actuation of these spools, i.e. release and accumulation of the slacks on the spools.

In order to avoid any undesired forward movement, a nonbackdrivable worm gear pair is used between the motors and spools. This prevents any forward force formed by the actuators to overcome the holding torque of the motors. Since worm gears have high reduction ratios and step motors are not able to work at high speeds, the spools

are actuated using brushless DC motors (BLDC). Maxon EC-i 30 BLDC motors are used at the system. Nominal speed and torque of these motors are 7030 rpm and 63.8 mNm, respectively. Framo Morat A25U40 worm gear set is used in this mechanism. They have a reduction ratio of 40:1 and center distance of 25 mm. Data sheets of BLDC motors and worm gear pair are given in Appendix.

The motors are connected to a shaft via a coupler, and the worm is mounted on this shaft. The worm gear on the other hand is connected to a shaft perpendicular to one of the worm. The spool is fixed to this shaft. Two ball bearings are used to retain and correctly center the spool and central shaft. A CAD image of this actuation mechanism can be seen in Figure 3.13. Overall design consists of three of the same mechanism. They are positioned around the colonoscope shaft in a circular pattern with 120° angle between them. Figure 3.14 shows assembly of the overall tubing feed mechanism. Each tubing is controlled individually with a separate BLDC motor. By adjusting speeds of the motors respectively, control of orientation and propagation of the colonoscope is achieved. Release speed of a tubing with respect to motor speed is given by Equation 3.7.

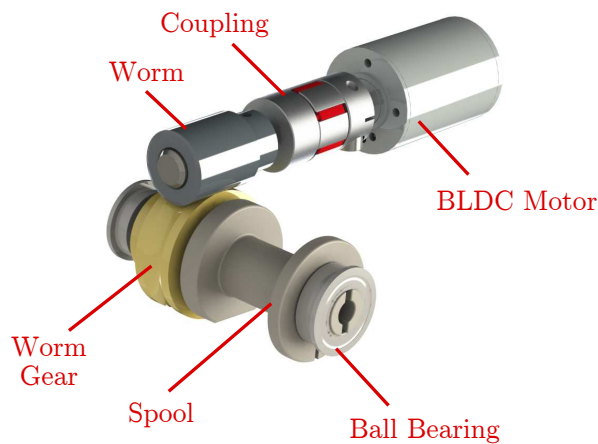


Figure 3.13. Actuation mechanism of the tubing feed.

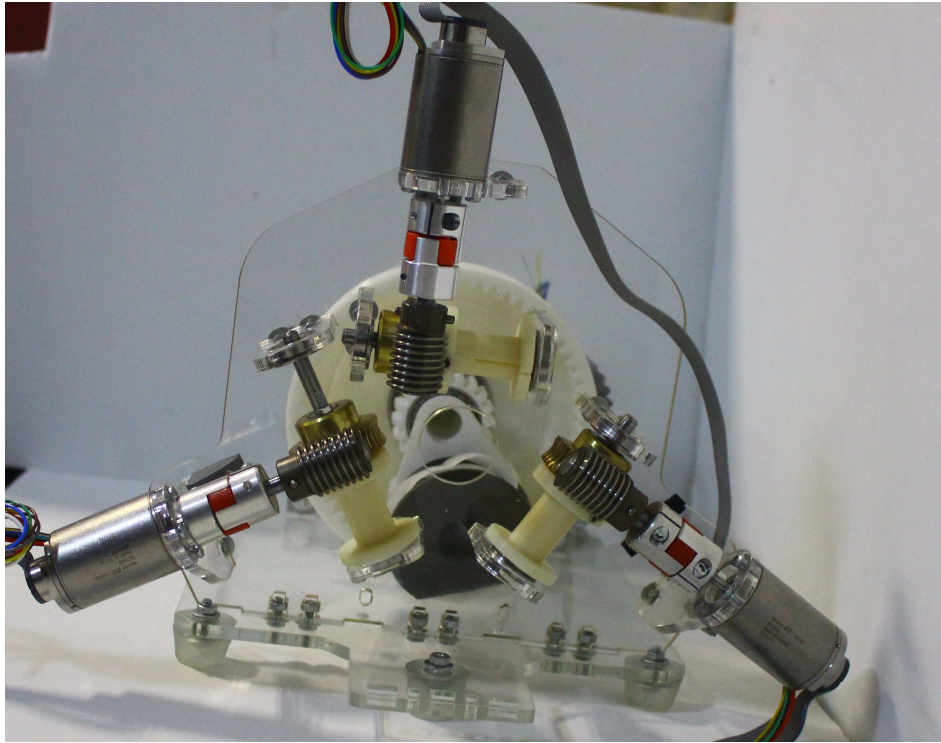


Figure 3.14. A picture of the manufactured tubing feed mechanism.

$$v_{t_i} = \frac{\omega_{t_i} r \pi}{i 60} \quad (3.7)$$

where v_{t_i} is release speed of i^{th} tubing in mm/s, ω_{t_i} is motor speed of i^{th} tubing in rpm, i is the reduction ratio of gear and r is the radius of the spool in mm. Since $i = 40$ and $r = 15$ mm v_{t_i} is found as:

$$v_{t_i} = \frac{\pi}{160} \omega_{t_i} \quad (3.8)$$

3.4.1.2. Shell Feed. The shell wraps around the inflated section of the tubings for reinforcement against buckling. While it is accumulated on top of the tubings, it should not make a twist motion and also should not need to be pulled from the tip. This may cause dramatic force losses and halt the motion. For this purpose, a planetary

gear system was designed. The system consists of a standard planetary gear set with specific tooth numbers. But none of the components is anchored and two actuators are used to control the feeding. Both the sun gear and carrier are actuated using stepper motors. The reason for such use is that it was desired to achieve different speed ratios between the carrier and planet gear.

The design is constructed around two hollow shafts connected to the sun gear and carrier. The inner shaft is connected to the carrier and actuated by a step motor. The outer one is connected to a sun gear and is also actuated similarly. Power transmission is obtained via gear and pinion pairs between the shafts and motors. The ring gear is free to rotate. The spool, in which the shell is accumulated, is connected to a planet gear and is not free to rotate with respect to it. By adjusting speeds and direction of the sun gear and carrier, rotation and direction of this spool is controlled. A schematic of this gear train is given in Figure 3.15.

Since the spool is connected to the planet gear, rotational speed of this gear should be calculated with respect to input speeds. The sun gear and carrier are actuated by step motors via gear and pinion couples with reduction ratios of 1:1 and 1.5:1, respectively. So it could be written as:

$$\omega_c = \omega_{s_1} \quad (3.9)$$

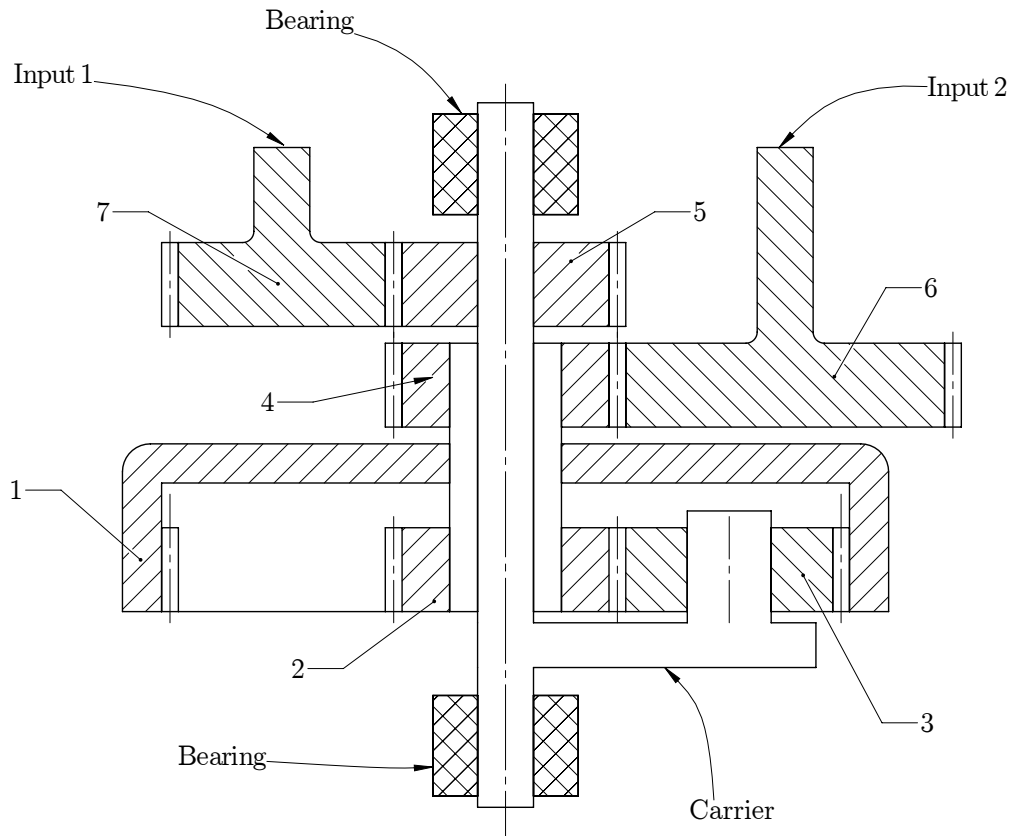
$$\omega_s = 1.5\omega_{s_2} \quad (3.10)$$

From Figure 3.16, speeds of point A and point B could written as follows.

$$v_A = \omega_s r_s = \omega_c (r_s + r_p) - \omega_p r_p \quad (3.11)$$

$$r_r = r_s + 2r_p \quad (3.12)$$

$$v_B = \omega_r (r_s + 2r_p) = \omega_c (r_s + r_p) + \omega_p r_p \quad (3.13)$$



- | | |
|------------------------------|----------------------------------|
| 1: Ring Gear, N=60 | 5: Carrier Connection Gear, N=20 |
| 2: Sun Gear, N=20 | 6: Sun Actuation Gear, N=30 |
| 3: Planet Gear, N=20 | 7: Carrier Actuation Gear, N=20 |
| 4: Sun Connection Gear, N=20 | |

Figure 3.15. Planetary gear train of the shell feed mechanism. Each gear is shown and described and tooth numbers are given. Note that module of every gear is 2.

Thus, from Equations 3.11 and 3.13, ω_r and ω_p values can be found.

$$\omega_p = \left(1 + \frac{r_s}{r_p}\right)\omega_c - \frac{r_s}{r_p}\omega_s \quad (3.14)$$

$$\omega_r = \frac{r_s + r_p}{r_p}\omega_c + \frac{r_s}{r_p}\omega_s \quad (3.15)$$

The helix shell should not apply any torsion on the colonoscope body. While feeding, it should not rotate around its axis. In order to feed the shell correctly as described, the planet gear should not rotate about its own axis of rotation. Since all the gears in the assembly have the same module, radii can be replaced with tooth

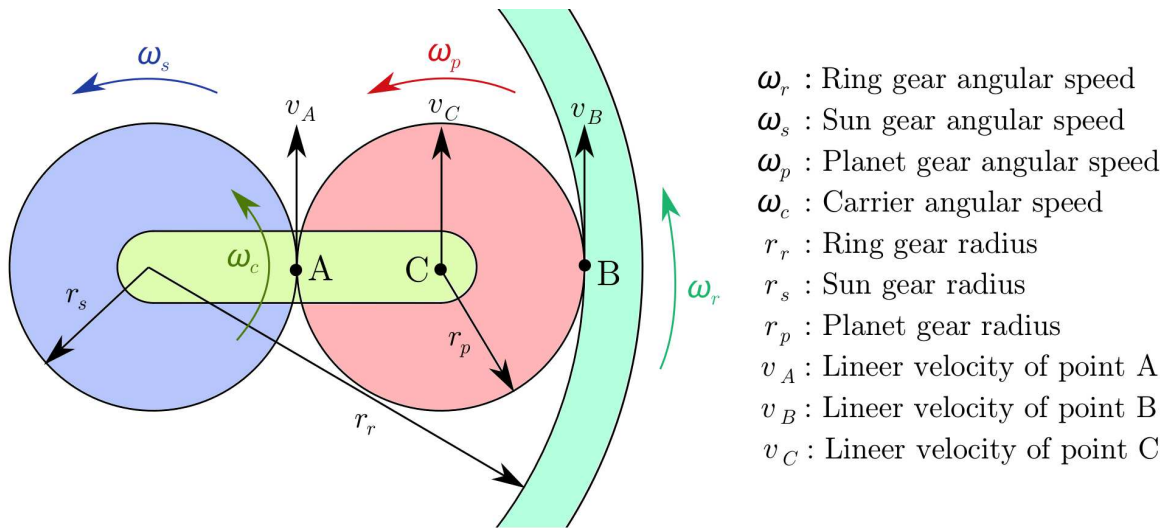


Figure 3.16. Planetary gear diagram describing aforementioned speeds.

number in equations. Substituting given tooth numbers in Figure 3.15 and input speeds of the motors we get the following relation for ω_{s_1} and ω_{s_2} .

$$\omega_{s_2} = \frac{4}{3}\omega_{s_1} \quad (3.16)$$

It is obvious that a more simpler system could be used with only one stepper motor. The reason for usage of two motors is to try different ratios with different planet rotation speeds. Also presence of a ring gear is redundant in the system in terms of speed control. But since the 3D printed carrier and its shaft has thin wall thicknesses (1.5 to 2.0 mm) it has low rigidity. Presence of the ring gear compensates this lack of rigidity for better operation of gears.

The gear train is fixed via the bearing around the sun gear shaft. Bearings are used for centering and correct placement of gears (See Figure 3.17). Stepper motors are also anchored using two vertical bases for them. The spool is mounted on the planet gear using a setscrew. Connection gears are also mounted to the stepper motors in the same fashion. Linear slipping of the gears are prevented using retaining rings.

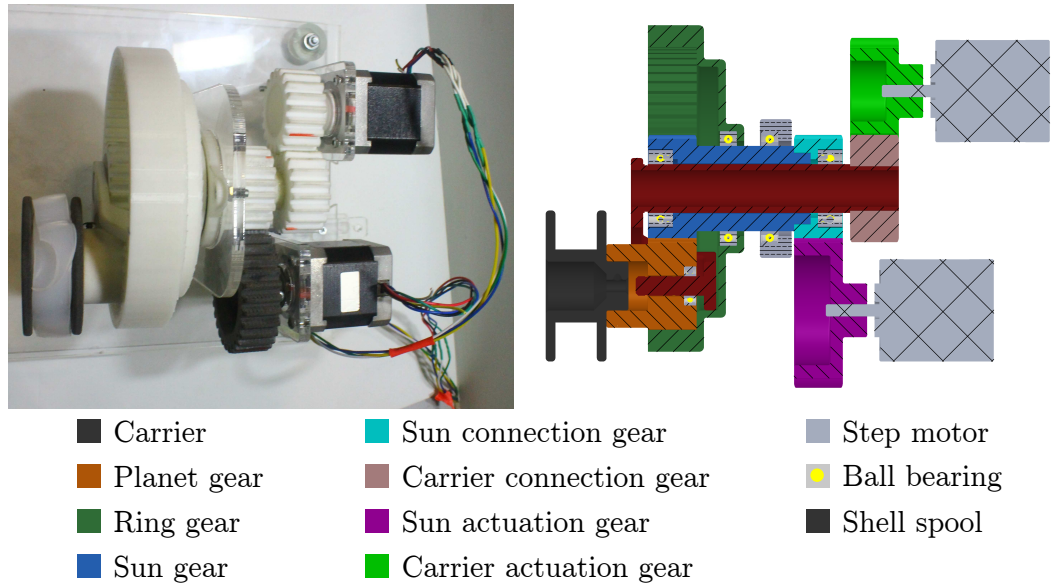


Figure 3.17. Prototype of the final shell feed mechanism and the design of the planetary gear train. Stepper motors and spool are also shown.

Linear speed of the shell depends directly on angular speed of the carrier, which is directly actuated by a motor. The other actuated component is the sun gear but it only ensures zero angular speed of the planet gear for the mechanism to feed the shell correctly, i.e. without torsion. Since the planet gear does not rotate on its own axis, one full rotation of the carrier causes the shell to wrap around the shaft one time. Since it is a pre-stressed helix structure, this makes it move forward at an amount equal to its pitch. Thus, its linear speed can be written as in Equation 3.17.

$$v_{shell} = \frac{p_{shell}\omega_c}{60} \quad (3.17)$$

where v_{shell} is linear speed of shell in mm/s, p_{shell} is the pitch of helix structure in mm and ω_c is angular speed of the carrier, i.e. shell spool, in rpm.

A kinematic model of the 3-DOF actuator is developed in a parallel study [83]. According to this study, total backbone length (l_b) and released tubing lengths (l_1 , l_2 and l_3) are found using Equations 3.18 to 3.21 [83].

$$l_b = \frac{1}{\kappa_b}(\pi - 2\theta) \quad (3.18)$$

$$l_1 = \left(\frac{1}{\kappa_b} - \sin \phi \left(\frac{a\sqrt{3}}{3} \right) \right) (\pi - 2\theta) \quad (3.19)$$

$$l_2 = \left(\frac{1}{\kappa_b} - \sin(\phi - 4\pi/3) \left(\frac{a\sqrt{3}}{3} \right) \right) (\pi - 2\theta) \quad (3.20)$$

$$l_3 = \left(\frac{1}{\kappa_b} - \sin(\phi - 2\pi/3) \left(\frac{a\sqrt{3}}{3} \right) \right) (\pi - 2\theta) \quad (3.21)$$

where κ_b is the backbone curvature, θ is the angle between z' -axis and diagonal of the backbone, ϕ is the rotation angle of backbone with respect to y-axis and a is the distance between tubing centers. Adding Equations 3.19 to 3.21 and substituting Equation 3.18 it is found that;

$$l_b = \frac{l_1 + l_2 + l_3}{3} \quad (3.22)$$

as expected since tubings are placed in a circular pattern having 120° spacing.

This implies that for a desired orientation and length of the colonoscope, speed of the carrier should be as given in Equation 3.23.

$$v_b = \frac{v_1 + v_2 + v_3}{3} \quad (3.23)$$

Substituting v_{shell} for v_b and using Equations 3.17 and 3.8; we get:

$$\omega_{s_1} = (\omega_{t_1} + \omega_{t_2} + \omega_{t_3}) \frac{\pi}{8p_{shell}} \quad (3.24)$$

3.4.1.3. Sheath Feed. The sheath adds up to the system lastly. As mentioned in Section 3.3.2.1, it has very low bending and axial stiffness. Taking advantage of this

fact, a simple base was designed for the sheath from where it can be fed when pulled from the tip. Similarly when the motors retract the system, the sheath is retracted in its base, accumulated around a three-piece hollow shaft. The sheath has a very high extension ratio and does require little space to accumulate.

To release the sheath in a more controlled fashion, three parts are designed around the base. These have slightly lower diameter at the tip of the base. This smaller dimension ensures that the sheath will be released when folded parts straighten out at a certain amount. Otherwise, when pulled, the sheath extends continuously as a whole. This makes the outer diameter of the overall system variable throughout the operation and cause differences in orientation control, since the slacks should not be in their exact planned path.

Outer diameter of the sheath differs before and after feeding. At its folded form, it has a diameter of 21 mm. But when released, it contracts and diameter drops in between 13-18 mm (see Figure 3.9). For this reason the diameter of central base is 20 mm. At the tip of circumferential releasers, diameter drops down to 16 mm.



Figure 3.18. An image of the sheath reservoir and feed. Flexible sheath is released when its diameter is reduced to a certain value via axial force.

3.4.2. Pneumatic System

The 3-DOF PRD uses pressurized air to exert forward force and control the orientation. Pressurized air should be controlled in order to supply the desired motion. Pressure is regulated using solenoid valves and pressure transmitters. A silent air compressor including a pressure vessel supplies the pressurized air.

Pressure of three tubings are controlled using one inlet valve, one exhaust valve and one pressure transmitter per tubing. It is also possible to adjust pressure with PWM control of the solenoid valves and transmitter. Figure 3.19 shows an image of the assembled pneumatic system.

Pressurized air from the pressure vessel is divided to three tubings using a 4-way pneumatic fitting. The inlet valves at each tubing control the inflation, and the exhaust valves deflate the air way when needed. After the exhaust valves, a pressure transmitter for each tubing are included for closed loop pressure control.

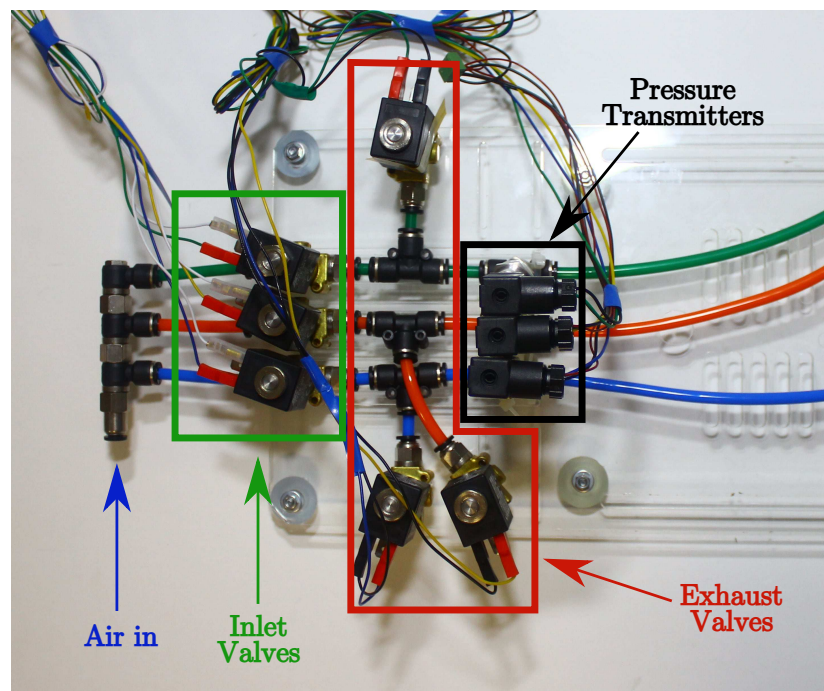


Figure 3.19. Assembly of the pneumatic system.

3.4.3. Control System

A basic control system and user interface for the colonoscope is developed. Control schematic of the overall system is given in Figure 3.20. NI CompactRIO Real-Time Controller (cRIO) is used for the control of the motors and inlet/exhaust valves. BLDC motors in the tubing feed mechanism are controlled using three Maxon 466023 ESCON Module 24/2 driver board and three Maxon Encoder 16 EASY encoders. Stepper motors are controlled using two A4988 DMOS Microstepping Driver. NPN type of bipolar junction transistors are used as switches for the control of the valves.

Control schematic is implemented in LabVIEW software (NI Inc.) to communicate with cRIO and its modules. Also a graphical user interface (GUI) is developed in the same software (see Figure 3.21). The system can be controlled in both manual and automatic modes once gear and spool ratios are adjusted in the GUI. In the manual mode every motor's speed is entered, and motors are enabled individually. Both inlet and exhaust valves are also opened or closed individually. On the other hand, in the automatic mode, the direction of the tip advancement is chosen, and the system adjusts speeds of the motors and states of the valves.

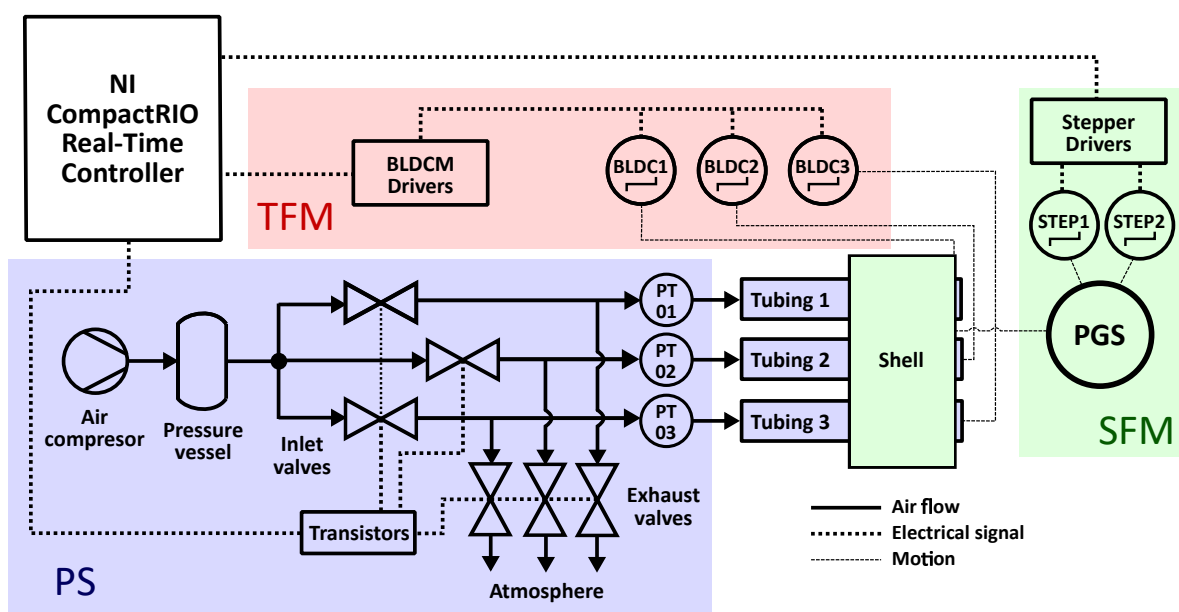


Figure 3.20. Schematic of the control system.

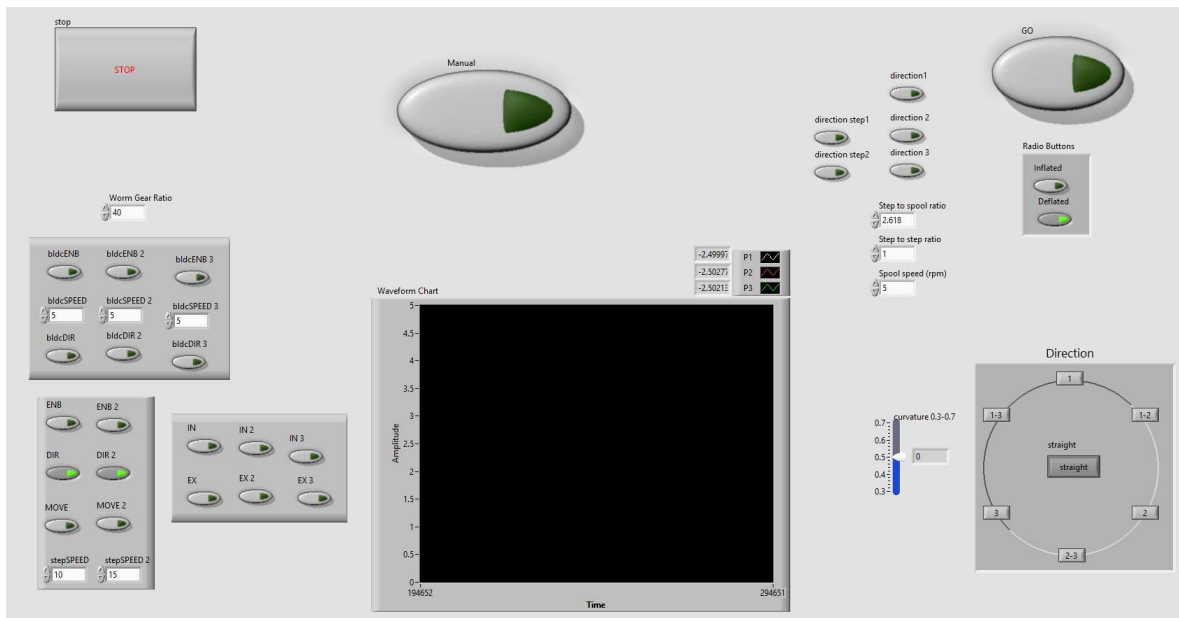


Figure 3.21. Graphical user interface of the system.

4. RESULTS AND DISCUSSION

The developed colonoscope is presented, and its performance in terms of actuation, stiffness, and navigation capabilities are discussed in this section. The developed GUI and control system are used for tests.

4.1. Actuator Performance

A 3-DOF PRD with an OD of 16.50 mm has been manufactured and assembled. Different tubings with diameter of 3 mm were obtained from two different manufacturers. The material for both of them is PA 12 but one of them has a Pebax inner layer. Double layered PA 12/Pebax tubings have a length of 2 m and manufactured via extrusion by Zeus Inc. Inner Pebax layer has a Shore 30D hardness and a wall thickness of 0.064 mm. Since its inner layer is soft, it has the ability to seal the air flow when the tubing is squeezed in between the rollers of the PRD. Outer PA 12 layer has a wall thickness of 0.038 mm and Shore 75D hardness. It restricts the tubing to expand radially and increases the burst pressure dramatically. On the other hand, PA 12 only tubings were manufactured by Simeks Inc. as catheter balloons. Therefore, they have

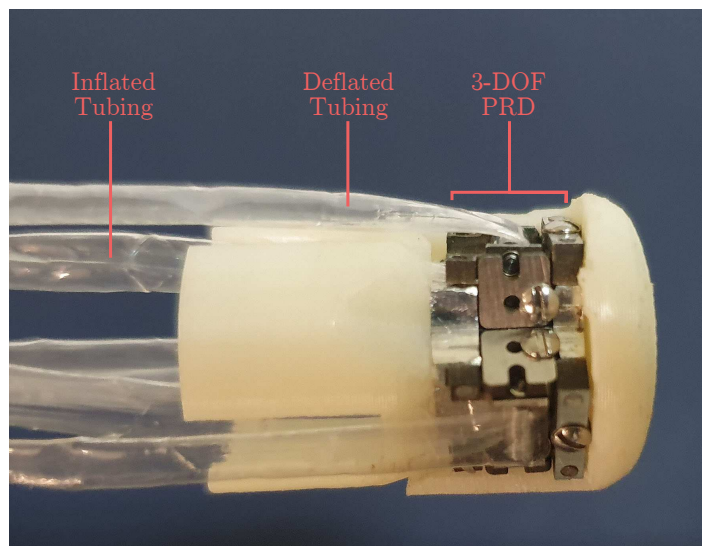


Figure 4.1. Miniaturized 3-DOF PRD with 2 meter long double layered tubings.

limited length (220 mm in this case). The manufacturer is not able to produce longer tubings because the necessary tooling is not present in their inventory.

Both tubings were tried with manufactured 3-DOF PRD. The double layered tubings were not able to produce any force output at the tip due to their incorrect wall thickness values of the manufactured tubings. The desired overall wall thickness was 102 μm , whereas wall thickness of the manufactured tubings was 165 μm (see Figure 4.2). Especially the thickness of the PA 12 layer causes the tubings to have high rigidity. Overall, the tubings are too hard for this application, and were not able to be bent without any buckling. On the other hand, for the catheter balloons, sealing between the rollers was not achieved due to high hardness value of PA. Even so, a force output was obtained when they were used in the 3-DOF PRD. This concludes that, the manufactured 3-DOF PRD works as intended. However, the desired tubing system was not obtained from any manufacturer.

Force output of the 3-DOF PRD was estimated as 3.85 N at 300 kPa pressure. But the force can be boosted to higher levels by increasing pressure. Even though tubings can withstand high pressures up to 800 kPa, air leakage between the rollers and yielding of the rollers are likely to happen at such pressures. Therefore, high levels of pressure is not applicable at these dimensions of the colonoscope shaft.



Figure 4.2. Thickness of the manufactured double layered tubings. Wall thickness corresponds to half of the value read (165 μm) since two layers of wall is measured.

4.2. Stiffness and Bending Capabilities

Stiffness of the body could be controlled using the shell feed mechanism. This capability of the shell is beneficial for avoiding loop formations of the colon. If the shell is fed when the tubings are held stationary, stiffness of the shell increases due to reduction of the spacing between coils of the helical shell (see Figure 4.3). Stiffness of the body can also be increased when the tubings are drawn back and the shell is kept stationary. But in this case, the tip is retracted by the axial contraction of the shell.

A high bending capability of the body was observed without any buckling behavior. This was tested when the body is passed through a rigid plexiglass pipe as shown in Figure 4.4. Free section of the body (from the end of the pipe to the tip) was bent using the tubing feed mechanism. The tubings were used in a cable driven system manner. While one of the tubings, which is at the inner side of the curvature, is drawn back, other two were kept stationary. The results showed that the body was able to bend 180° angle without any buckling (see Figure 4.4). It is demonstrated that high angle turns are possible when the body has support from the inner side of the turn.

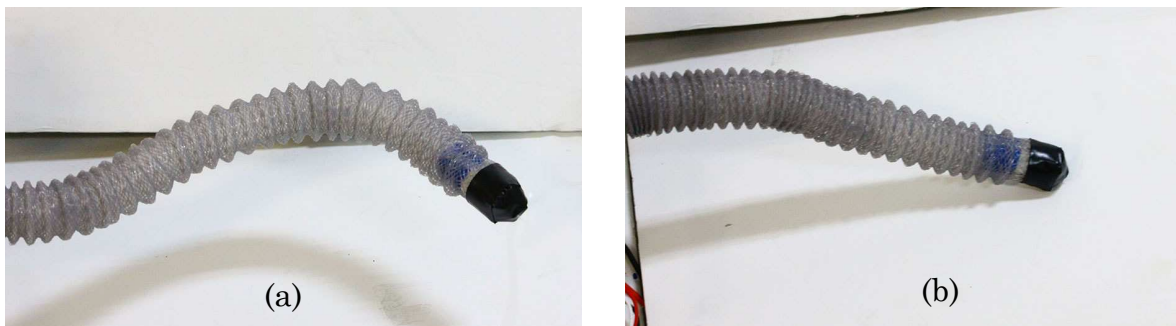


Figure 4.3. The body at a certain tubing configuration with non-inflated 2 meter long double layered tubings when the shell is stiffened (a), and the body when the shell is in free state (b).

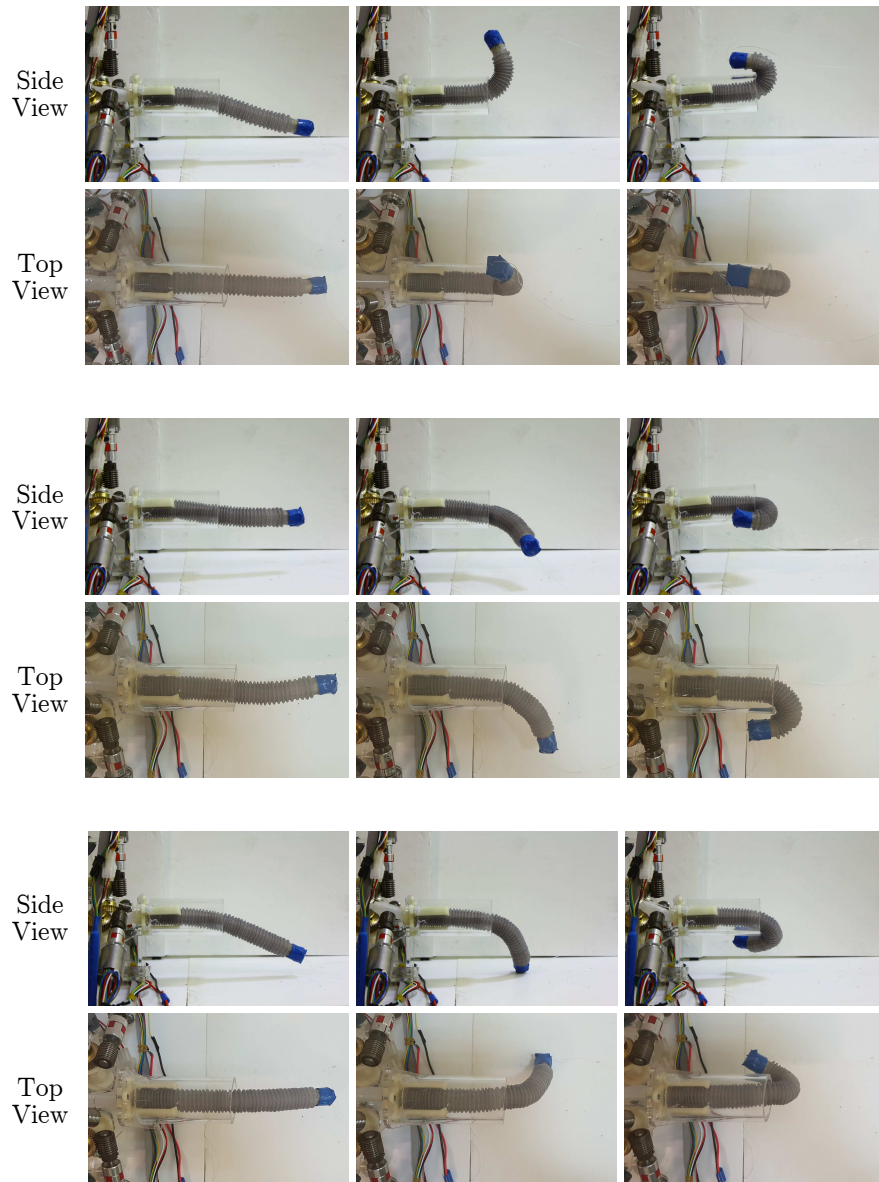


Figure 4.4. 180° bending of the body actuated in a tendon-driven fashion via slack tubings at the end of a rigid tube. Three different orientations in 3D space can be seen.

4.3. Navigation Capability

As mentioned in Section 4.1, the long tubings were not able to produce any force while the catheter balloons were too short to be used in the current prototype. Thus, the colonoscope body could not be tested thoroughly. Instead, a test setup is developed to observe the operation of the feed mechanisms. Since a force output was not formed

at the tip by the 3-DOF PRD, the axial force was supplied manually by hand using a tendon (see Figure 4.5).

Overall, the tubing and shell feed mechanisms are observed to work synchronously. Speed of the tip is efficiently controlled when the axial force is supplied. It is also observed that the withdrawal of the system is achieved without any buckling behavior of the shaft at low speeds.

When actuated as explained in Section 3.4.1, the helical shell advanced with minimal torsion. Small amounts of torsion was observed in the shell due to its imperfections originating from its elastic nature. The helical pitch and outer diameter of the shell cannot preserve its original form. Small differences in these dimensions lead to errors in both axial speed and torsional immobility. On the other hand, spool diameter does not affect speed or torsion of the shell as expected.

Speed of the tip and bending of the body is controlled via the tubing feed mechanism. Some errors in speed are present due to change in release radius during operation. Compatibility issues were observed between the tubing feed and shell feed for this reason. The maximum error in speed is expected to be about 20%, since the accumulation of the tubings does not exceed 3 mm while OD of the spool is 30 mm. This did not cause problems in bending since all three of them are released at the same time with small differences while the shaft is bent.

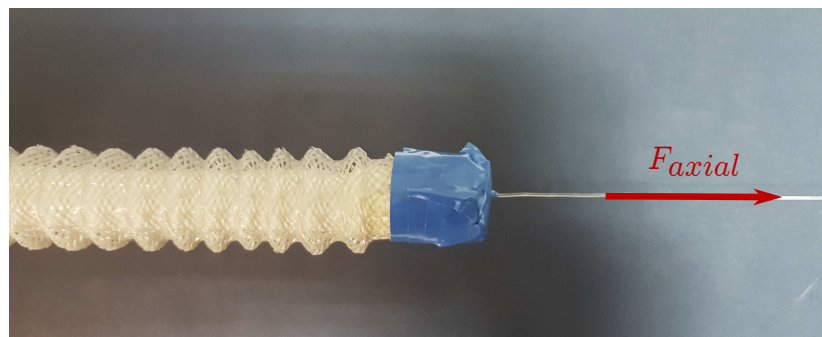


Figure 4.5. Manually applied axial force using a tendon connected through the center-line of the 3-DOF PRD.

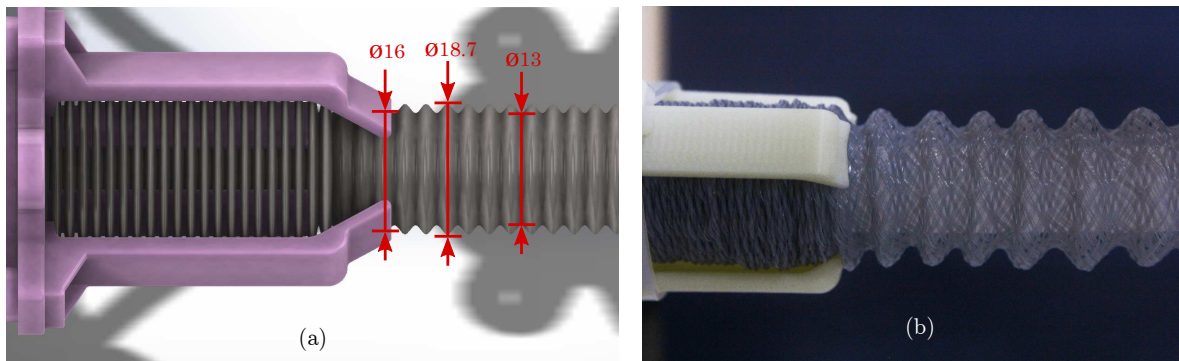


Figure 4.6. (a) Minimum/maximum outer diameters of the sheath after feeding, and release diameter of the reservoir. Dimensions are in mm. (b) A picture of the prototype at the same configuration.

The sheath reservoir is able to release the the outer sheath as desired when the axial force is applied. The release diameter of the sheath is set to be 16 mm so that friction with the slack tubings could be minimal. The minimum and maximum OD of the sheath are 13 mm and 18.7 mm respectively (see Figure 4.6).

The developed colonoscope body was tested inside an enclosed rigid tube. The entrance of the tubing was placed at approximately 40 mm higher than the initial position of the tip and at a 15° horizontal angle (see Figure 4.7). Since the actuators did not work with the long tubings, the axial force was supplied manually parallel to the shaft's center-line using a tendon. This test showed the ability of the body to navigate inside an enclosed tube. Using the feed mechanisms, the orientation of the body is controlled as desired.

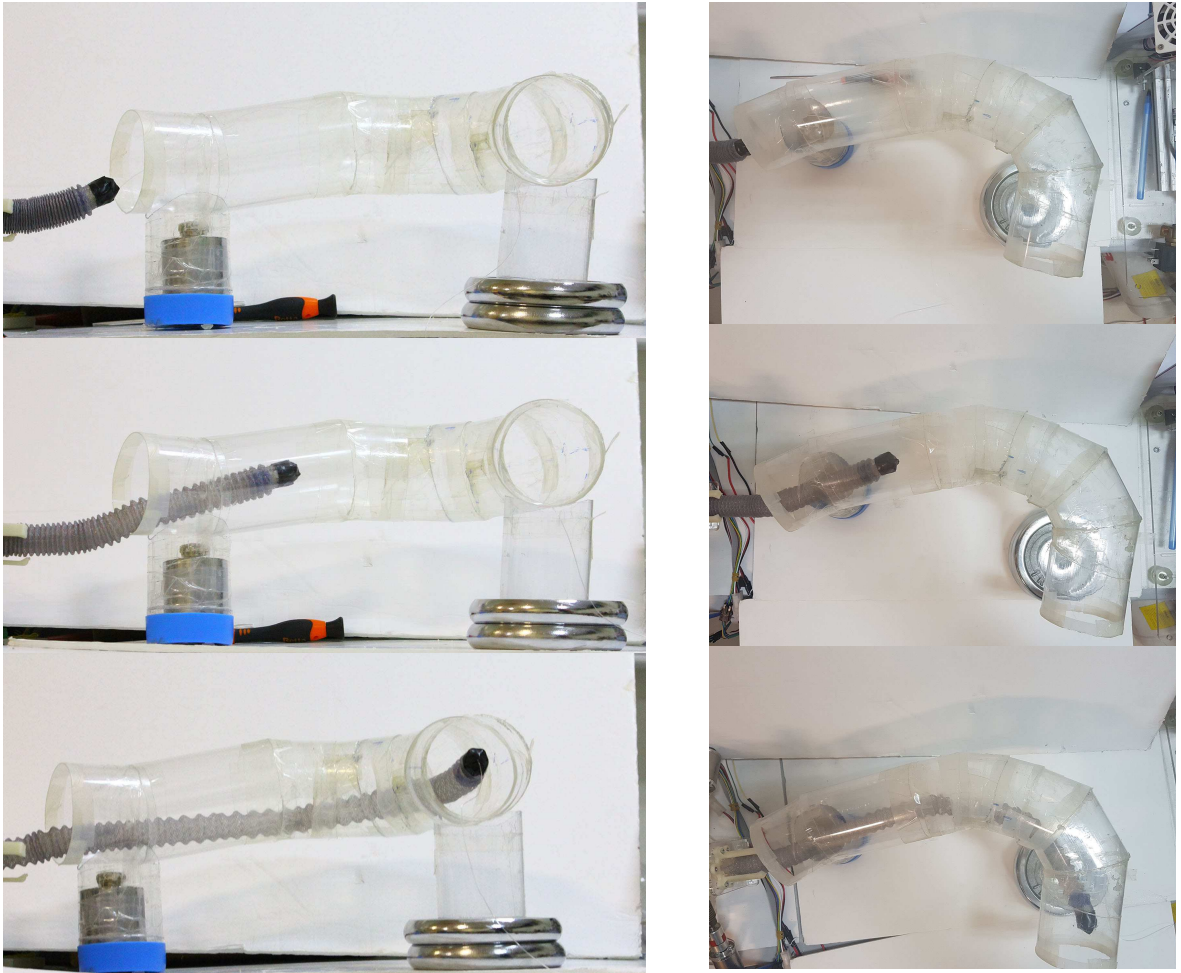


Figure 4.7. Advancement of the colonoscope in an enclosed tube.

5. CONCLUSION

In this study, a novel design for an extensible colonoscope is presented. A prototype, including feed mechanisms (*in-vitro* section) has been developed. The prototype was observed in different circumstances and configurations for different performance outputs of the colonoscope body.

The proposed design consists of three layers of concentric parts which are positioned around a novel actuator. These parts accumulate at the *in-vitro* section by means of three feed mechanisms. The feed mechanisms feed the parts of the colonoscope on top of each other in a concentric fashion. Qualitative observations showed that the proposed design is able to advance in an enclosed path, adjust its stiffness and bend at high angles and low radii of curvature in 3D space. The maximum outer diameter of the colonoscope is 18 mm. The only rigid part of this dimension is due to sheath retainer at the tip. This retention mechanism can be included into the base of 3-D0F PRD and the OD can be reduced to 16.2 mm. Overall length of the prototype is approximately 70 cm, but this can be increased up to 2 meters since used parts are available at higher lengths.

5.1. Contributions and Originality

The proposed colonoscope body is actuated from the tip. Unlike conventional colonoscopes, the axial force is supplied from the tip by means of pulling. When the tip of the body is bent, the direction of the forward force is controlled too. Thus, the force applied to the colon wall could be reduced significantly, reducing possible complications of colonoscopy.

A poster presentation about the conceptual design was made in the Hamlyn Symposium on Medical Robotics 2018 [76]. Another poster presentation was made in Turkey Robotics Conference (TORK) 2018. Also, an article has been submitted to

the Soft Robotics journal about the large-scale prototype framed as a pneumatic soft growing robot [74].

5.2. Outlook and Future Work

The proposed colonoscope can be advantageous over conventional colonoscopes in many ways. However, there are some aspects of the prototype which needs improvement. Firstly, the 3-DOF PRD can work as intended with tubings which are manufactured more precisely on the needed wall thicknesses. Also, the feed mechanisms and retention of the colonoscope parts should be made in a more rigid and robust way for more precise operation. Feeding of the shell could be made better with a new helical structure, smoother surface and uniform wall thickness. The outer sheath used in the prototype is permeable. This should be replaced with a similar structure using an unpermeable material.

With an advanced control algorithm and precisely manufactured tubings, a to-be-developed colonoscopy robot could advance with minimal pressure on the colon wall. This pressure exerted on the wall should be measured in an *in-vitro* test setup. Incompatibility between the tubing feed and shell feed mechanisms should be calibrated by reducing the release speed of the shell with respect to the amount of released tubings. Also with more advanced *in-vitro* section design and better manufacturing of the parts in *in-vivo* section, the control of robot would be easier and more precise. Visual systems, air/CO₂ channels and illumination should be implemented on the tip. Cabling and tubing is possible through the colonoscope with the existing design. All the parts should be manufactured using medically compatible materials for any *in-vivo* experiments.

Since the pneumatic actuator has a capability to advance at high speeds, CI times under 10 minutes are expected. Also, since the actuation is supplied from the tip, high CI rates are anticipated. As a different approach; the tip can advance to cecum in short times and screening of the colon can be done during the withdrawal of the colonoscope, since the retraction speeds are lower compared to forward advancement speeds.

REFERENCES

1. Gandomani, H. S., S. M. Yousefi, M. Aghajani, A. Mohammadian-Hafshejani, A. A. Tarazoj, V. Pouyesh and H. Salehiniya, “Colorectal cancer in the world: incidence, mortality and risk factors”, *Biomedical Research and Therapy*, Vol. 4, No. 10, p. 1656, oct 2017.
2. Ferlay, J., I. Soerjomataram, R. Dikshit, S. Eser, C. Mathers, M. Rebelo, D. M. Parkin, D. Forman and F. Bray, “Cancer incidence and mortality worldwide: Sources, methods and major patterns in GLOBOCAN 2012”, *International Journal of Cancer*, Vol. 136, No. 5, pp. E359–E386, mar 2015.
3. Edwards, B. K., E. Ward, B. A. Kohler *et al.*, “Annual report to the nation on the status of cancer, 1975-2006, featuring colorectal cancer trends and impact of interventions (risk factors, screening, and treatment) to reduce future rates”, *Cancer*, Vol. 116, No. 3, pp. 544–573, feb 2010.
4. Rex, D. K., P. S. Schoenfeld, J. Cohen, I. M. Pike, D. G. Adler, B. M. Fennerty, J. G. Lieb, W. G. Park, M. K. Rizk, M. S. Sawhney, N. J. Shaheen, S. Wani and D. S. Weinberg, “Quality Indicators for Colonoscopy”, *American Journal of Gastroenterology*, Vol. 110, No. 1, pp. 72–90, jan 2015.
5. John Hopkins Medicine, *Colonoscopy*, 2018, <https://www.hopkinsmedicine.org/gastroenterology/hepatology/clinical/services/basic/endoscopy/colonoscopy.html>, accessed in July 2019.
6. Wolff, W. I. and H. Shinya, “Colonofiberoscopy.”, *JAMA*, Vol. 217, No. 11, pp. 1509–12, sep 1971.
7. Lee, S.-H., Y.-K. Park, D.-J. Lee and K.-M. Kim, “Colonoscopy procedural skills and training for new beginners.”, *World journal of gastroenterology*, Vol. 20, No. 45,

- pp. 16984–95, dec 2014.
8. Brooker, J. C., B. P. Saunders, S. G. Shah and C. B. Williams, “A new variable stiffness colonoscope makes colonoscopy easier: A randomised controlled trial”, *Gut*, Vol. 46, No. 6, pp. 801–805, jun 2000.
 9. Barclay, R. L., J. J. Vicari and R. L. Greenlaw, “Effect of a Time-Dependent Colonoscopic Withdrawal Protocol on Adenoma Detection During Screening Colonoscopy”, *Clinical Gastroenterology and Hepatology*, Vol. 6, No. 10, pp. 1091–1098, oct 2008.
 10. Jain, D., A. Goyal and S. Zavala, “Predicting Colonoscopy Time: A Quality Improvement Initiative”, *Clinical Endoscopy*, Vol. 49, No. 6, pp. 555–559, nov 2016.
 11. Witte, T. N. and R. Enns, “The Difficult Colonoscopy”, *Canadian Journal of Gastroenterology*, Vol. 21, No. 8, pp. 487–490, aug 2007.
 12. PENTAX Medical, *i10 Series Video Colonoscopes*, 2019, <http://www.pentaxmedical.com/pentax/en/95/1/i10-Series-Video-Colonoscopes/>, accessed in July 2019.
 13. Mitchell, R. M. S., K. McCallion, K. R. Gardiner, R. G. P. Watson and J. S. A. Collins, “Successful colonoscopy; completion rates and reasons for incompleteness.”, *The Ulster medical journal*, Vol. 71, No. 1, pp. 34–7, may 2002.
 14. Eickhoff, A., P. J. Pickhardt, D. Hartmann and J. F. Riemann, “Colon anatomy based on CT colonography and fluoroscopy: Impact on looping, straightening and ancillary manoeuvres in colonoscopy”, *Digestive and Liver Disease*, Vol. 42, No. 4, pp. 291–296, apr 2010.
 15. Geyer, M., U. Guller and C. Beglinger, “Carbon dioxide insufflation in routine colonoscopy is safe and more comfortable: Results of a randomized controlled double-blinded trial”, *Diagnostic and Therapeutic Endoscopy*, Vol. 2011, 2011.

16. Janssens, F., J. Deviere, P. Eisendrath and J. M. Dumonceau, “Carbon dioxide for gut distension during digestive endoscopy: Technique and practice survey”, *World Journal of Gastroenterology*, Vol. 15, No. 12, pp. 1475–1479, 2009.
17. Kahai, P., P. Mandiga and S. Lobo, *Anatomy, Abdomen and Pelvis, Large Intestine*, StatPearls Publishing, Treasure Island (FL), 2019.
18. Avgerinos, D. V., O. H. Llaguna, A. Y. Lo and I. M. Leitman, “Evolving management of colonoscopic perforations”, *Journal of Gastrointestinal Surgery*, Vol. 12, No. 10, pp. 1783–1789, oct 2008.
19. Agarwal, A., *Large Intestine*, 2018, <https://www.knowyourbody.net/large-intestine.html>, accessed in July 2019.
20. Levin, T. R., W. Zhao, C. Conell, L. C. Seeff, D. L. Manninen, J. A. Shapiro and J. Schulman, “Complications of Colonoscopy in an Integrated Health Care Delivery System”, *Annals of Internal Medicine*, Vol. 145, No. 12, p. 880, dec 2006.
21. Fisher, D. A., J. T. Maple, T. Ben-Menachem, B. D. Cash, G. A. Decker, D. S. Early, J. A. Evans, R. D. Fanelli, N. Fukami, J. H. Hwang, R. Jain, T. L. Jue, K. M. Khan, P. M. Malpas, R. N. Sharaf, A. K. Shergill and J. A. Dornitz, “Complications of colonoscopy”, *Gastrointestinal Endoscopy*, Vol. 74, No. 4, pp. 745–752, oct 2011.
22. Castro, G., M. F. Azrak, L. C. Seeff and J. Royalty, “Outpatient colonoscopy complications in the CDC’s Colorectal Cancer Screening Demonstration Program”, *Cancer*, Vol. 119, No. SUPPL. 15, pp. 2849–2854, aug 2013.
23. Waye, J. D., O. Kahn and M. E. Auerbach, “Complications of colonoscopy and flexible sigmoidoscopy.”, *Gastrointestinal endoscopy clinics of North America*, Vol. 6, No. 2, pp. 343–77, apr 1996.
24. Gatto, N. M., H. Frucht, V. Sundararajan, J. S. Jacobson, V. R. Grann and A. I.

- Neugut, “Risk of Perforation After Colonoscopy and Sigmoidoscopy: A Population-Based Study”, *JNCI: Journal of the National Cancer Institute*, Vol. 95, No. 3, pp. 230–236, jun 2003.
25. Anderson, M. L., T. M. Pasha and J. A. Leighton, “Endoscopic perforation of the colon: lessons from a 10-year study.”, *The American journal of gastroenterology*, Vol. 95, No. 12, pp. 3418–22, dec 2000.
26. Damore, L. J., P. C. Rantis, A. M. Vernava and W. E. Longo, “Colonoscopic perforations. Etiology, diagnosis, and management.”, *Diseases of the colon and rectum*, Vol. 39, No. 11, pp. 1308–14, nov 1996.
27. Joseph, D. A., R. G. S. Meester, A. G. Zauber, D. L. Manninen, L. Wings, F. B. Dong, B. Peaker and M. van Ballegooijen, “Colorectal cancer screening: Estimated future colonoscopy need and current volume and capacity”, *Cancer*, Vol. 122, No. 16, pp. 2479–2486, aug 2016.
28. Raju, G. S., D. K. Rex, R. A. Kozarek, I. Ahmed, D. Brining and P. J. Pasricha, “A novel shape-locking guide for prevention of sigmoid looping during colonoscopy”, *Gastrointestinal Endoscopy*, Vol. 59, No. 3, pp. 416–419, mar 2004.
29. Cheng, W. B., M. A. Moser, S. Kanagaratnam and W. J. Zhang, “Overview of Upcoming Advances in Colonoscopy”, *Digestive Endoscopy*, Vol. 24, No. 1, pp. 1–6, jan 2012.
30. Saunders, B., F. Macrae and C. Williams, “What makes colonoscopy difficult?”, *Gut*, Vol. 34, No. A181, 1993.
31. Ruffolo, T. A., G. A. Lehman and D. Rex, “Colonoscope damage from internal straightener use.”, *Gastrointestinal endoscopy*, Vol. 37, No. 1, pp. 107–8, 1991.
32. Tierney, W. M., D. G. Adler, J. D. Conway, D. L. Diehl, F. A. Farraye, S. V. Kantsevov, V. Kaul, S. R. Kethu, R. S. Kwon, P. Mamula, M. C. Pedrosa and

- S. A. Rodriguez, "Overtube use in gastrointestinal endoscopy", *Gastrointestinal Endoscopy*, Vol. 70, No. 5, pp. 828–834, nov 2009.
33. Shah, S. G., J. C. Brooker, C. Thapar, C. B. Williams and B. P. Saunders, "Patient pain during colonoscopy: an analysis using real-time magnetic endoscope imaging.", *Endoscopy*, Vol. 34, No. 6, pp. 435–40, jun 2002.
34. Yoshikawa, I., H. Honda, K. Nagata, K. Kanda, T. Yamasaki, K. Kume, A. Tabaru and M. Otsuki, "Variable stiffness colonoscopes are associated with less pain during colonoscopy in unsedated patients.", *The American journal of gastroenterology*, Vol. 97, No. 12, pp. 3052–5, dec 2002.
35. Sorbi, D., C. D. Schleck, A. R. Zinsmeister and C. J. Gostout, "Clinical application of a new colonoscope with variable insertion tube rigidity: A pilot study", *Gastrointestinal Endoscopy*, Vol. 53, No. 6, pp. 638–642, may 2001.
36. Hewett, D. G. and D. K. Rex, "Cap-fitted colonoscopy: a randomized, tandem colonoscopy study of adenoma miss rates", *Gastrointestinal Endoscopy*, Vol. 72, No. 4, pp. 775–781, oct 2010.
37. A. Mir, F., "Cap-assisted colonoscopy versus standard colonoscopy: is the cap beneficial? A meta-analysis of randomized controlled trials", *Annals of Gastroenterology*, Vol. 30, jan 2017.
38. DeMarco, D. C., E. Odstreil, L. F. Lara, D. Bass, C. Herdman, T. Kinney, K. Gupta, L. Wolf, T. Dewar, T. M. Deas, M. K. Mehta, M. B. Anwer, R. Pellish, J. K. Hamilton, D. Polter, K. G. Reddy and I. Hanan, "Impact of experience with a retrograde-viewing device on adenoma detection rates and withdrawal times during colonoscopy: the Third Eye Retroscope study group", *Gastrointestinal Endoscopy*, Vol. 71, No. 3, pp. 542–550, mar 2010.
39. Gralnek, I. M., "Emerging technological advancements in colonoscopy: Third

- Eye® Retroscope® and Third Eye® Panoramic TM , Fuse® Full Spectrum Endoscopy® colonoscopy platform, Extra-Wide-Angle-View colonoscope, and NaviAid TM G-EYE TM balloon colonoscope”, *Digestive Endoscopy*, Vol. 27, No. 2, pp. 223–231, jan 2015.
40. Rubin, M., L. Lurie, K. Bose and S. H. Kim, “Expanding the view of a standard colonoscope with the Third Eye ® Panoramic™ cap”, *World Journal of Gastroenterology*, Vol. 21, No. 37, p. 10683, 2015.
41. Dik, V. K., L. M. Moons and P. D. Siersema, “Endoscopic innovations to increase the adenoma detection rate during colonoscopy”, *World Journal of Gastroenterology*, Vol. 20, No. 9, p. 2200, 2014.
42. Yung, D. E., E. Rondonotti and A. Koulaouzidis, “Review: capsule colonoscopy—a concise clinical overview of current status”, *Annals of Translational Medicine*, Vol. 4, No. 20, pp. 398–398, 2016.
43. Schoofs, N., J. Devière and A. Van Gossum, “PillCam colon capsule endoscopy compared with colonoscopy for colorectal tumor diagnosis: a prospective pilot study”, *Endoscopy*, Vol. 38, No. 10, pp. 971–977, oct 2006.
44. Van Gossum, A., M. Munoz-Navas, I. Fernandez-Urien, C. Carretero, G. Gay, M. Delvaux, M. G. Lapalus, T. Ponchon, H. Neuhaus, M. Philipper, G. Costamagna, M. E. Riccioni, C. Spada, L. Petruzzello, C. Fraser, A. Postgate, A. Fitzpatrick, F. Hagenmuller, M. Keuchel, N. Schoofs and J. Devière, “Capsule Endoscopy versus Colonoscopy for the Detection of Polyps and Cancer”, *New England Journal of Medicine*, Vol. 361, No. 3, pp. 264–270, jul 2009.
45. Spada, C., C. Hassan, R. Marmo, L. Petruzzello, M. E. Riccioni, A. Zullo, P. Cesaro, J. Pilz and G. Costamagna, “Meta-analysis Shows Colon Capsule Endoscopy Is Effective in Detecting Colorectal Polyps”, *Clinical Gastroenterology and Hepatology*, Vol. 8, No. 6, pp. 516–522.e8, jun 2010.

46. Spada, C., C. Hassan, M. Munoz-Navas, H. Neuhaus, J. Deviere, P. Fockens, E. Coron, G. Gay, E. Toth, M. E. Riccioni, C. Carretero, J. P. Charton, A. Van Gossum, C. A. Wientjes, S. Sacher-Huvelin, M. Delvaux, A. Nemeth, L. Petruzzello, C. P. de Frias, R. Mayershofer, L. Aminejab, E. Dekker, J.-P. Galmiche, M. Frederic, G. W. Johansson, P. Cesaro and G. Costamagna, “Second-generation colon capsule endoscopy compared with colonoscopy”, *Gastrointestinal Endoscopy*, Vol. 74, No. 3, pp. 581–589.e1, sep 2011.
47. Han, Y. M. and J. P. Im, “Colon Capsule Endoscopy: Where Are We and Where Are We Going”, *Clinical Endoscopy*, Vol. 49, No. 5, pp. 449–453, sep 2016.
48. Spada, C., M. E. Riccioni, C. Hassan, L. Petruzzello, P. Cesaro and G. Costamagna, “PillCam colon capsule endoscopy: a prospective, randomized trial comparing two regimens of preparation”, *Journal of Clinical Gastroenterology*, Vol. 45, No. 2, pp. 119–124, feb 2011.
49. Hong, S. N., S.-H. Kang, H. J. Jang and M. B. Wallace, “Recent Advance in Colon Capsule Endoscopy: What’s New?”, *Clinical Endoscopy*, Vol. 51, No. 4, pp. 334–343, jul 2018.
50. Adrián-de Ganzo, Z., O. Alarcón-Fernández, L. Ramos, A. Gimeno-García, I. Alonso-Abreu, M. Carrillo and E. Quintero, “Uptake of Colon Capsule Endoscopy vs Colonoscopy for Screening Relatives of Patients With Colorectal Cancer”, *Clinical Gastroenterology and Hepatology*, Vol. 13, No. 13, pp. 2293–2301.e1, dec 2015.
51. Morris, B., “Robotic surgery: applications, limitations, and impact on surgical education.”, *MedGenMed : Medscape general medicine*, Vol. 7, No. 3, p. 72, sep 2005.
52. Speich, J. E. and J. Rosen, “Medical Robotics”, *Encyclopedia of Biomaterials and Biomedical Engineering*, April, pp. 983–993, Marcel Dekker, Inc., New York, NY,

- 2004.
53. Dsouza, R., C. Deborah, V. Samuel and A. Sunaina, “Evolution of Robotics in Medical Surgeries and Health Care Systems A Review”, *International Journal of Applied Engineering Research*, Vol. 11, pp. 11277–11298, 2016.
 54. Vitiello, V., S. L. Lee, T. P. Cundy and G. Z. Yang, “Emerging robotic platforms for minimally invasive surgery”, *IEEE Reviews in Biomedical Engineering*, Vol. 6, No. December, pp. 111–126, 2013.
 55. Bergeles, C. and Guang-Zhong Yang, “From Passive Tool Holders to Microsurgeons: Safer, Smaller, Smarter Surgical Robots”, *IEEE Transactions on Biomedical Engineering*, Vol. 61, No. 5, pp. 1565–1576, may 2014.
 56. U.S. National Library of Medicine, *Endoscopy*, 2019, <https://medlineplus.gov/endoscopy.html>, accessed in July 2019.
 57. Robinson, G. and J. Davies, “Continuum robots - a state of the art”, *Proceedings 1999 IEEE International Conference on Robotics and Automation (Cat. No.99CH36288C)*, Vol. 4, pp. 2849–2854, IEEE, 1999.
 58. Johnson, P. J., C. M. R. Serrano, M. Castro, R. Kuenzler, H. Choset, S. Tully and U. Duvvuri, “Demonstration of transoral surgery in cadaveric specimens with the medrobotics flex system”, *The Laryngoscope*, Vol. 123, No. 5, pp. 1168–1172, may 2013.
 59. Degani, A., H. Choset, A. Wolf and M. Zenati, “Highly articulated robotic probe for minimally invasive surgery”, *Proceedings 2006 IEEE International Conference on Robotics and Automation, 2006. ICRA 2006.*, pp. 4167–4172, IEEE, 2006.
 60. Slatkin, A. B., J. Burdick and W. Grundfest, “The development of a robotic endoscope”, O. Khatib and J. K. Salisbury (Editors), *Experimental Robotics IV*, pp. 161–169, Springer Berlin Heidelberg, 1997.

61. Cosentino, F., E. Tumino, G. Rubis, A. Rigante, R. Barbera, A. Tauro and P. Emanuel, “Robotic Colonoscopy”, *Colonoscopy*, InTech, aug 2011.
62. Grattagliano, I., C. Tosetti, E. Ubaldi and C. Cricelli, “Comments to “The intelligent, painless, “germ-free” colonoscopy: A Columbus’ egg for increasing population adherence to colorectal cancer screening?””, *Digestive and Liver Disease*, Vol. 43, No. 10, pp. 836–837, oct 2011.
63. Cosentino, F., E. Tumino, G. R. Passoni, E. Morandi and A. Capria, “Functional evaluation of the Endotics System, a new disposable self-propelled robotic colonoscope: In vitro tests and clinical trial”, *International Journal of Artificial Organs*, Vol. 32, No. 8, pp. 517–527, 2009.
64. Tumino, E., R. Sacco, M. Bertini, M. Bertoni, G. Parisi and A. Capria, “Endotics system vs colonoscopy for the detection of polyps”, *World Journal of Gastroenterology*, Vol. 16, No. 43, pp. 5452–5456, 2010.
65. Eickhoff, A., R. Jakobs, A. Kamal, S. Mermash, J. Riemann and J. van Dam, “In vitro evaluation of forces exerted by a new computer-assisted colonoscope (the NeoGuide Endoscopy System)”, *Endoscopy*, Vol. 38, No. 12, pp. 1224–1229, dec 2006.
66. Van Dam, J., A. Eickhoff, R. Jakobs, V. Kudis, D. Hartmann and J. F. Riemann, “Computer-Assisted Colonoscopy (the NeoGuide System): Results of the First Human Clinical Trial”, *Gastrointestinal Endoscopy*, Vol. 63, No. 5, p. AB100, apr 2006.
67. Eickhoff, A., J. Van Dam, R. Jakobs, V. Kudis, D. Hartmann, U. Damian, U. Weickert, D. Schilling and J. F. Riemann, “Computer-assisted colonoscopy (the NeoGuide Endoscopy System): Results of the first human clinical trial (“PACE Study”)”, *American Journal of Gastroenterology*, Vol. 102, No. 2, pp. 261–266, 2007.

68. Gluck, N., A. Melhem, Z. Halpern, K. Mergener and E. Santo, “A novel self-propelled disposable colonoscope is effective for colonoscopy in humans (with video)”, *Gastrointestinal Endoscopy*, Vol. 83, No. 5, pp. 998–1004.e1, may 2016.
69. Vucelic, B., D. Rex, R. Pulanic, J. Pfefer, I. Hrstic, B. Levin, Z. Halpern and N. Arber, “The Aer-O-Scope: Proof of Concept of a Pneumatic, Skill-Independent, Self-Propelling, Self-Navigating Colonoscope”, *Gastroenterology*, Vol. 130, No. 3, pp. 672–677, mar 2006.
70. Shike, M., Z. Fireman, R. Eliakim, O. Segol, A. Sloyer, L. B. Cohen, S. Goldfarb-Albak and A. Repici, “Sightline ColonoSight system for a disposable, power-assisted, non-fiber-optic colonoscopy (with video)”, *Gastrointestinal Endoscopy*, Vol. 68, No. 4, pp. 701–710, 2008.
71. Rösch, T., A. Adler, H. Pohl, E. Wettschureck, M. Koch, B. Wiedenmann and N. Hoepffner, “A motor-driven single-use colonoscope controlled with a hand-held device: a feasibility study in volunteers”, *Gastrointestinal Endoscopy*, Vol. 67, No. 7, pp. 1139–1146, 2008.
72. Groth, S., D. K. Rex, T. Rösch and N. Hoepffner, “High cecal intubation rates with a new computer-assisted colonoscope: A feasibility study”, *American Journal of Gastroenterology*, Vol. 106, No. 6, pp. 1075–1080, 2011.
73. Baydere, B. A., *Design of a Highly-Extensible Pneumatic Actuator for Soft Robotic Applications*, Master’s thesis, Boğaziçi University, 2019.
74. Baydere, B. A., S. K. Talas and E. Samur, “A novel highly-extensible 2-DOF pneumatic actuator for soft robotic applications”, *Sensors and Actuators A: Physical*, Vol. 281, pp. 84–94, oct 2018.
75. Talas, S. K., B. A. Baydere, T. Altinsoy, C. Tutcu and E. Samur, “Design and Development of a Growing Pneumatic Soft Robot”, *Soft Robotics*, In Review.

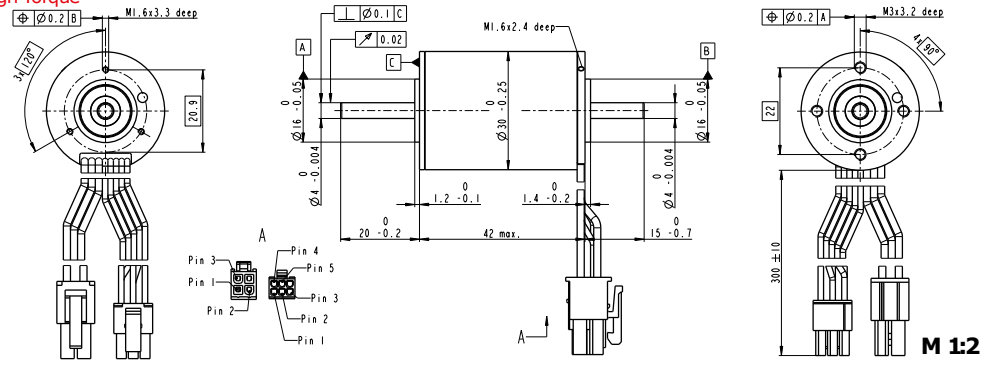
76. Altinsoy, T., B. A. Baydere, S. K. Talas, O. M. Erkan, C. Tutcu and E. Samur, “Design of an Extensible Colonoscopy Robot”, *The Hamlyn Symposium on Medical Robotics*, pp. 25–26, The Hamlyn Centre, Faculty of Engineering, Imperial College London, jun 2018.
77. Talas, S. K., *Control System Design of a Highly-Extensible Soft Continuum Robot*, Master’s thesis, Boğaziçi University, 2019.
78. Varadarajulu, S., S. Banerjee, B. A. Barth, D. J. Desilets, V. Kaul, S. R. Kethu, M. C. Pedrosa, P. R. Pfau, J. L. Tokar, A. Wang, L.-M. Wong Kee Song and S. A. Rodriguez, “GI endoscopes”, *Gastrointestinal Endoscopy*, Vol. 74, No. 1, pp. 1–6.e6, jul 2011.
79. ASM Aerospace Specification Metals Inc., “Aluminum 7075-T6; 7075-T651”, <http://asm.matweb.com/search/SpecificMaterial.asp?bassnum=MA7075T6>, accessed in July 2019.
80. ASM Aerospace Specification Metals Inc., “AISI Type 304 Stainless Steel”, <http://asm.matweb.com/search/SpecificMaterial.asp?bassnum=MQ304A>, accessed in July 2019.
81. ASM Aerospace Specification Metals Inc., “AISI Type 302 Stainless Steel, cold rolled to 1140 MPa tensile strength”, <http://asm.matweb.com/search/SpecificMaterial.asp?bassnum=MQ302AF>, accessed in July 2019.
82. ASM International. Handbook Committee, *Properties and Selection: Nonferrous Alloys and Special- Purpose Materials*, ASM International, 1990.
83. Tutcu, C., B. A. Baydere, S. K. Talas and E. Samur, “Quasi-static Modeling of a Novel Growing Soft-Continuum Robot”, *International Journal of Robotics Research*, In Review.

APPENDIX A: DATASHEETS

EC-i 30 Ø30 mm, brushless, 45 Watt

High Torque

maxon EC-i



		Part Numbers				
		539480	539481	539482	539483	539484
with Hall sensors						
Motor Data (provisional)						
Values at nominal voltage						
1 Nominal voltage	V	12	18	24	36	48
2 No load speed	rpm	8250	8250	8520	8250	8520
3 No load current	mA	273	182	143	91.1	71.5
4 Nominal speed	rpm	6710	6760	7030	6790	7050
5 Nominal torque (max. continuous torque)	mNm	65.4	67.7	63.8	67.6	63.8
6 Nominal current (max. continuous current)	A	4.51	3.09	2.28	1.54	1.14
7 Stall torque	mNm	731	840	811	885	835
8 Stall current	A	53.2	40.8	30.5	21.5	15.7
9 Max. efficiency	%	86.3	87.2	86.9	87.5	87.1
Characteristics						
10 Terminal resistance phase to phase	Ω	0.225	0.441	0.787	1.68	3.06
11 Terminal inductance phase to phase	mH	0.199	0.449	0.749	1.8	3
12 Torque constant	mNm/A	13.7	20.6	26.6	41.2	53.2
13 Speed constant	rpm/V	696	464	359	232	180
14 Speed/torque gradient	rpm/mNm	11.4	9.94	10.6	9.43	10.3
15 Mechanical time constant	ms	0.969	0.843	0.902	0.8	0.876
16 Rotor inertia	gcm ²	8.1	8.1	8.1	8.1	8.1
Specifications		Operating Range				
Thermal data				Comments		
17 Thermal resistance housing-ambient	11.1 K/W			Continuous operation		
18 Thermal resistance winding-housing	3.75 K/W			In observation of above listed thermal resistance (lines 17 and 18) the maximum permissible winding temperature will be reached during continuous operation at 25°C ambient. = Thermal limit.		
19 Thermal time constant winding	27.8 s			Short term operation		
20 Thermal time constant motor	866 s			The motor may be briefly overloaded (recuring).		
21 Ambient temperature	-40...+100°C			Assigned power rating		
22 Max. winding temperature	+155°C					
Mechanical data (preloaded ball bearings)						
23 Max. speed	10000 rpm					
24 Axial play at axial load	< 9.0 N 0 mm > 9.0 N 0.14 mm preloaded					
25 Radial play	5 N					
26 Max. axial load (dynamic)	98 N					
27 Max. force for press f ts (static) (static, shaft supported)	2000 N					
28 Max. radial load, 5 mm from f range	25 N					
Other specifications						
29 Number of pole pairs	4					
30 Number of phases	3					
31 Weight of motor	156 g					
Values listed in the table are nominal.						
Connection motor (Cable AWG 20)						
red	Motor winding 1	Pin 1				
black	Motor winding 2	Pin 2				
white	Motor winding 3	Pin 3				
	N.C.	Pin 4				
Connector Article number						
Molex	39-01-2040					
Connection sensors (Cable AWG 26)						
yellow	Hall sensor 1	Pin 1				
brown	Hall sensor 2	Pin 2				
grey	Hall sensor 3	Pin 3				
blue	GND	Pin 4				
green	V _{ref} 4.5... 24 VDC	Pin 5				
	N.C.	Pin 6				
Connector Article number						
Molex	430-25-0600					
Wiring diagram for Hall sensors see p. 43						
maxon Modular System						
Planetary Gearhead		Spindle Drive		Recommended Electronics:		
Ø32 mm 1.0 - 6.0 Nm Page 339		Ø32 mm Page 366-368		Notes Page 32		
				ESCON 36/3 EC		
				ESCON Mod. 50/4 EC-S		
				ESCON Mod. 50/5		
				ESCON 50/5		
				DEC Module 50/5		
				EPOS2 Module 36/2		
				EPOS2 24/5		
				EPOS2 50/5		
				EPOS2 P 24/5		
				EPOS4 Mod./Comp. 50/5		
				MAXPOS 50/5		
				Encoder 16 EASY		
				128 - 1024 CPT, 3 channels		
				Page 395		
				Encoder 16 EASY Absolute		
				4096 steps		
				Page 396		
				Encoder 16 RID		
				1024 - 32768 CPT, 3 channels		
				Page 408		
				Encoder HEDL 5540		
				500 CPT, 3 channels		
				Page 418		
				Encoder AEDL 5810		
				1024 - 5000 CPT, 3 channels		
				Page 412		
November 2017 edition / subject to change						

Figure A.1. BLDC motor datasheet. Model with the number 539482 was used.

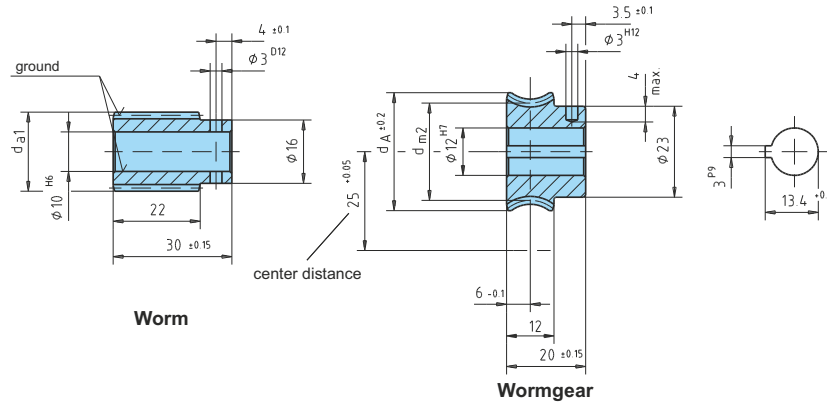
Worm gear sets



9

A25 (25 mm center distance)

METRIC



pressure angle 15°

- i = gear ratio
- γ_m = lead angle
- m = module
- z_1 = number of threads
- d_{m1} = pitch diameter (worm)
- d_{a1} = tip diameter (worm)
- z_2 = No. of teeth
- d_{m2} = pitch diameter (worm gear)
- d_A = max. diameter (worm gear)
- T_2 = output torque
- MG = mineral grease
- MO = mineral oil / synthetic grease
- SO = synthetic oil

Catalog	worm						wormgear			T ₂ [Nm] No.			
	i	γ_m	m	z ₁	d _{m1}	d _{a1}	z ₂	d _{m2}	d _A	Bronze			Phe-nolic
										MG	MO	SO	
A25U4	4:1	20°29'	1.4	5	20	22.8	20	30.0	33.5	5.1	6.1	7.6	2.0
A25U5	5:1	19°15'	1.5	4	18.2	21.2	20	31.8	34.8	6.5	7.8	9.7	2.6
A25U6	6.5:1	13°52'	1.15	4	19.2	21.5	26	30.8	34.8	6	7.2	9	2.4
A25U10	10:1	8°48'	1.5	2	19.6	22.6	20	30.4	34.8	5.9	7.1	8.8	2.4
A25U15	15:1	6°29'	1.0	2	17.7	19.7	30	32.3	34.8	5.7	6.8	8.5	2.3
A25U20	20:1	4°19'	1.5	1	19.9	22.9	20	30.1	34.8	5.8	7.0	8.7	2.3
A25U25	25:1	2°18'	1.0	1	24.96	26.96	25	25.04	27.8	4.1	4.9	6.1	1.6
A25U30	30:1	2°53'	1.0	1	19.9	21.9	30	30.1	33.5	5.9	7.1	8.8	2.4
A25U40	40:1	2°33'	0.8	1	17.96	19.56	40	32.04	34.8	6.2	7.4	9.3	2.5
A25U50	50:1	1°43'	0.6	1	19.96	21.16	50	30.04	33.5	5.1	6.1	7.6	2.0

All worms and worm gears stocked right hand only.
 Worm made of case hardened and ground steel (HV 620 - 700).
 Worm gear made of CuZn37Mn3Al2PbSi-S40 or at request of plastic or Hgw 2083.

Subject to technical changes

Framo Morat GmbH & Co. KG
 Franz-Morat-Straße 6 • D-79871 Eisenbach

Tel.: +49 (0) 7657 / 88-0
 Fax: +49 (0) 7657 / 88-333

www.framo-morat.com
 info@framo-morat.com

Figure A.2. Framo Morat worm gear set datasheet. Model with the number A25U40 was used.

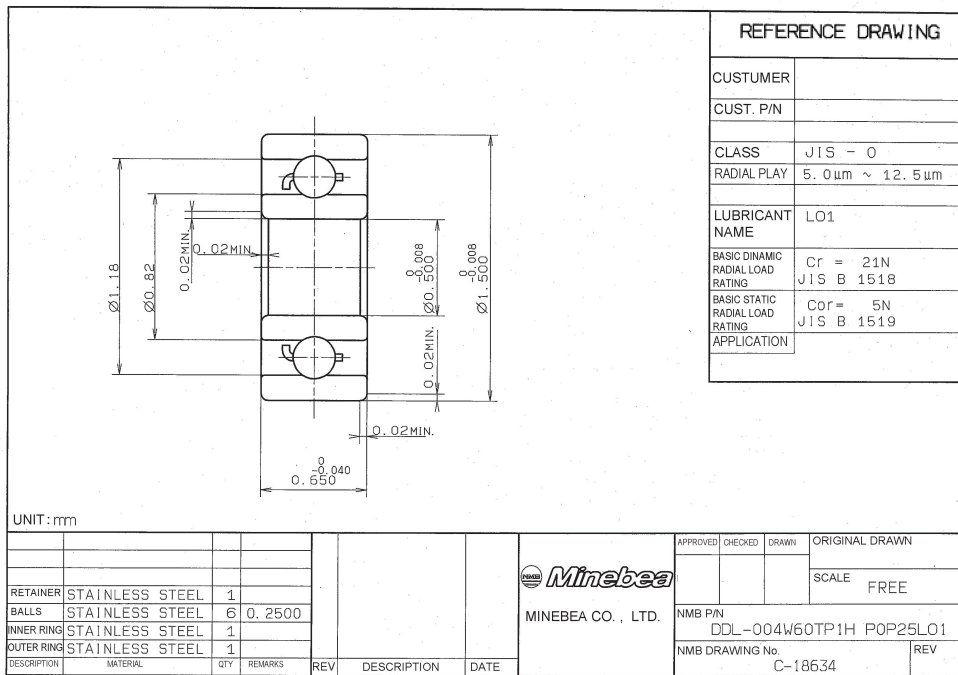


Figure A.3. Reference drawing of ball bearings used in 3-DOF PRD.

A4988

DMOS Microstepping Driver with Translator And Overcurrent Protection

Functional Block Diagram

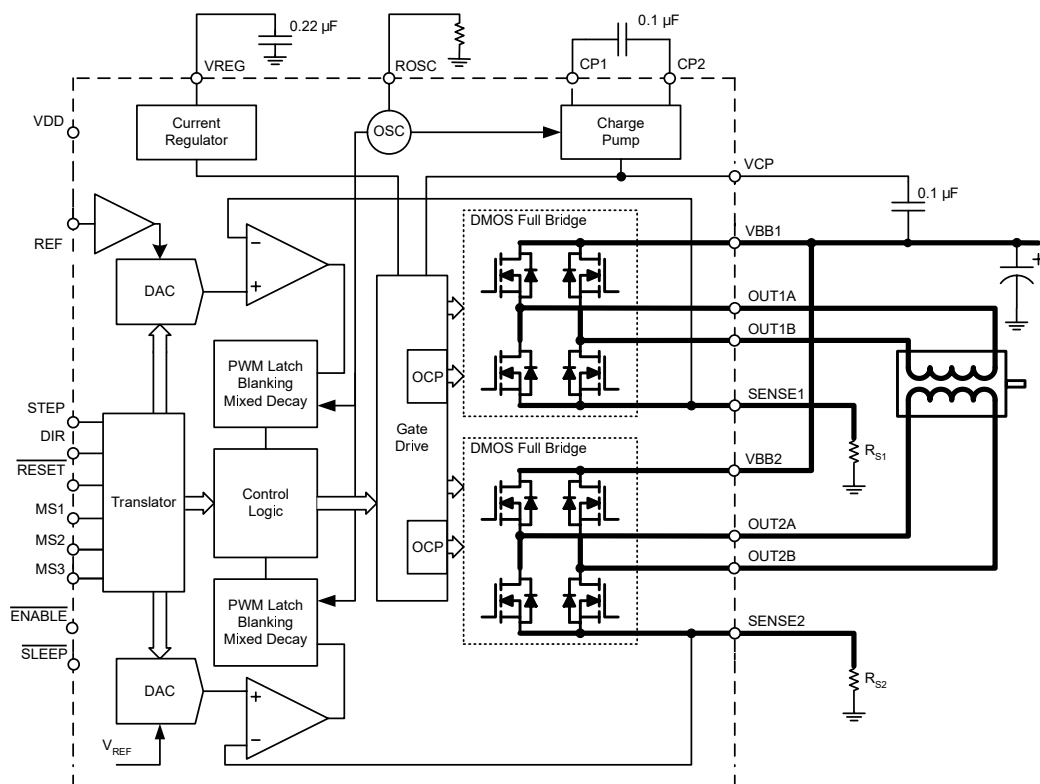


Figure A.4. Functional block diagram of A4988 stepper motor driver.

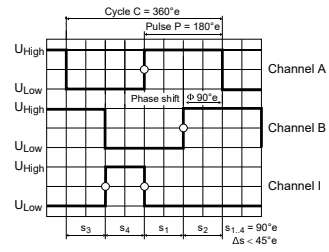
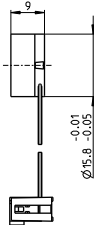
ESCON Feature Comparison Chart



	ESCON Module 24/2	ESCON 36/2 DC
DC motors up to (continuous / maximum)	48 W / 144 W	72 W / 144 W
EC motors up to (continuous / maximum)	48 W / 144 W	–
Sensors		
	Digital Incremental Encoder (2 channel with or without Line Driver)	Digital Incremental Encoder (2 channel with or without Line Driver)
	DC Tacho	DC Tacho
	Without sensor (DC motors)	Without sensor (DC motors)
	Digital Hall Sensors (EC motors)	–
Operating mode		
	Current controller (torque control), Speed controller (closed and open loop)	Current controller (torque control), Speed controller (closed and open loop)
Electrical data		
Nominal operating voltage V_{CC}	10 - 24 VDC	10 - 36 VDC
Max. output voltage	$0.98 \times V_{CC}$	$0.98 \times V_{CC}$
Max. output current	6 A (<4 s)	4 A (<60 s)
Continuous output current	2 A	2 A
Pulse width modulation frequency	53.6 kHz	53.6 kHz
Sampling rate PI current controller	53.6 kHz	53.6 kHz
Sampling rate PI speed controller	5.36 kHz	5.36 kHz
Max. efficiency	92%	95%
Max. speed (DC)	limited by max. speed (motor) and max. output voltage (controller)	limited by max. speed (motor) and max. output voltage (controller)
Max. speed (EC; 1 pole pair)	150 000 rpm	–
Built-in motor choke	–	300 μ H / 2 A
Inputs/Outputs		
Hall sensor signals	H1, H2, H3	–
Encoder signals	A, A\, B, B\	A, A\, B, B\
Max. encoder input frequency differential (single-ended)	1 MHz (100 kHz)	1 MHz (100 kHz)
Potentiometers	–	1
Digital inputs	2	2
Digital inputs/outputs	2	2
Analog inputs	2	2
Resolution, Range, Circuit	12-bit, -10... +10 V, differential	12-bit, -10... +10 V, differential
Analog outputs	2	2
Resolution, Range	12-bit, -4... +4 V	12-bit, -4... +4 V
Auxiliary voltage output	+5 VDC ($I_L \leq 10$ mA)	+5 VDC ($I_L \leq 10$ mA)
Hall sensor supply voltage	+5 VDC ($I_L \leq 30$ mA)	–
Encoder supply voltage	+5 VDC ($I_L \leq 70$ mA)	+5 VDC ($I_L \leq 70$ mA)
Status Indicators	Operation: green LED / Error: red LED	Operation: green LED / Error: red LED
Environmental conditions		
Temperature – Operation	-30... +60°C	-30... +45°C
Temperature – Extended range	+60... +80°C; Derating: -0.100 A/°C	+45... +81°C; Derating: -0.056 A/°C
Temperature – Storage	-40... +85°C	-40... +85°C
Humidity (condensation not permitted)	5... 90%	5... 90%
Mechanical data		
Weight	Approx. 7 g	Approx. 30 g
Dimensions (L x W x H)	35.6 x 26.7 x 12.7 mm	55.0 x 40.0 x 16.1 mm
Mounting holes	Plugable (socket headers with 2.54 mm pitch)	for screws M2.5
Part numbers		
	466023 ESCON Module 24/2	403112 ESCON 36/2 DC
	Order accessories separately, from page 437	Order accessories separately, from page 437

Figure A.5. Features of ESCON Module 24/2 BLDCM driver board.

Encoder 16 EASY 128–1024 CPT, 3 Channels, with Line Driver RS 422



Direction of rotation cw (definition cw p. 60)

maxon sensor

- Stock program
- Standard program
- Special program (on request)

Part Numbers

499356	499357	499358	499359	499360	499361
--------	--------	--------	--------	--------	--------

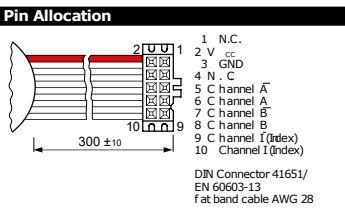
Type (provisional)	128	256	500	512	1000	1024
Counts per turn	128	256	500	512	1000	1024
Number of channels	3	3	3	3	3	3
Max. operating frequency (kHz)	200	400	800	800	1600	1600
Max. speed (rpm)	30000	30000	30000	30000	30000	30000
Phase shift φ (°e)	90 ± 45	90 ± 45	90 ± 60	90 ± 45	90 ± 80	90 ± 70
Index pulse width (°e)	90 ± 45	90 ± 45	90 ± 60	90 ± 45	90 ± 80	90 ± 70



maxon Modular System

+ Motor	Page	+ Gearhead	Page	+ Brake	Page	Overall length (mm)	see Gearhead			
EC-4pole 22, 90 W	237					60.8	60.8	60.8	60.8	60.8
EC-4pole 22, 90 W	237	GP 22/GP 32	329/339			•	•	•	•	•
EC-4pole 22, 90 W	237	GP 32 S	366-368			•	•	•	•	•
EC-4pole 22, 120 W	238					78.2	78.2	78.2	78.2	78.2
EC-4pole 22, 120 W	238	GP 22/GP 32	329/339			•	•	•	•	•
EC-4pole 22, 120 W	238	GP 32 S	366-368			•	•	•	•	•
EC-4pole 30, 100 W	239					60.9	60.9	60.9	60.9	60.9
EC-4pole 30, 100 W	239	GP 32, 4.0 - 8.0 Nm	341			•	•	•	•	•
EC-4pole 30, 100 W	239	GP 42, 3 - 15 Nm	346			•	•	•	•	•
EC-4pole 30, 100 W	239					•	•	•	•	•
EC-4pole 30, 100 W	239	GP 32, 4.0 - 8.0 Nm	341			•	•	•	•	•
EC-4pole 30, 100 W	239	GP 42, 3 - 15 Nm	346			•	•	•	•	•
EC-4pole 30, 200 W	241					77.9	77.9	77.9	77.9	77.9
EC-4pole 30, 200 W	241	GP 32, 4.0 - 8.0 Nm	341			•	•	•	•	•
EC-4pole 30, 200 W	241	GP 42, 3 - 15 Nm	346			•	•	•	•	•
EC-4pole 30, 200 W	241					•	•	•	•	•
EC-4pole 30, 200 W	241	GP 32, 4.0 - 8.0 Nm	341			•	•	•	•	•
EC-4pole 30, 200 W	241	GP 42, 3 - 15 Nm	346			•	•	•	•	•
EC-i 40, 50 W	247/248					37.7	37.7	37.7	37.7	37.7
EC-i 40, 50 W	247	GP 32, 1 - 6 Nm	339			•	•	•	•	•
EC-i 40, 50 W	247	GP 32 S	366-368			•	•	•	•	•
EC-i 40, 50 W	247/248	GP 42, 3 - 15 Nm	346			•	•	•	•	•
EC-i 40, 70 W	249/250					47.7	47.7	47.7	47.7	47.7
EC-i 40, 70 W	249	GP 32, 1 - 6 Nm	339			•	•	•	•	•
EC-i 40, 70 W	249	GP 32 S	366-368			•	•	•	•	•
EC-i 40, 70 W	249/250	GP 42, 3 - 15 Nm	346			•	•	•	•	•
EC-i 40, 100 W	251					67.7	67.7	67.7	67.7	67.7
EC-i 40, 100 W	251	GP 42, 3 - 15 Nm	346			•	•	•	•	•
EC-i 52, 180 W	252					93.7	93.7	93.7	93.7	93.7
EC-i 52, 180 W	252	GP 52, 4 - 30 Nm	354			•	•	•	•	•

Technical Data	
Supply voltage V _{cc}	5 V ± 10%
Typical current draw	22 mA
Output signal	EIA Standard RS 422
Operating temperature range	-40... +100 °C
Moment of inertia of code wheel	≤ 0.09 gcm ²
Output current per channel	± 20 mA
Hysteresis	0.17 °m
Min. state duration s	125 ns
Signal rise and fall times (typically, at C _i = 200 pF, R _L = 100 Ω)	20 ns
The angle value 0 is matched to the commutation phase of winding 1 (in acc. with Hall 1 signal on motors with Hall sensors, block commutation), see p. 40.	
Additional information can be found in the maxon online shop under downloads.	
The index signal I is synchronized with channel A or B.	



Option: also available in a single-strand version.

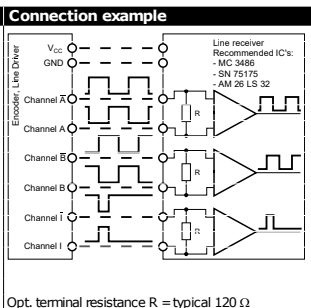


Figure A.6. Maxon BLDCM encoder datasheet.

APPENDIX B: TECHNICAL DRAWINGS

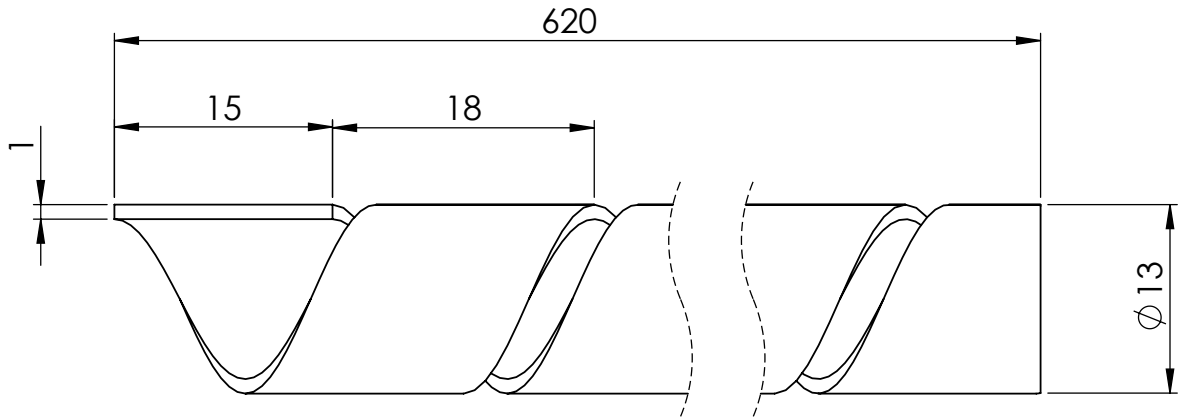


Figure B.1. Technical drawing of shell's helical structure. All dimensions are in mm.



Figure B.2. Technical drawing of 3-DOF PRD's rollers. D is 2.20 mm and 1.40 mm for outer and inner rollers respectively. All dimensions are in mm.

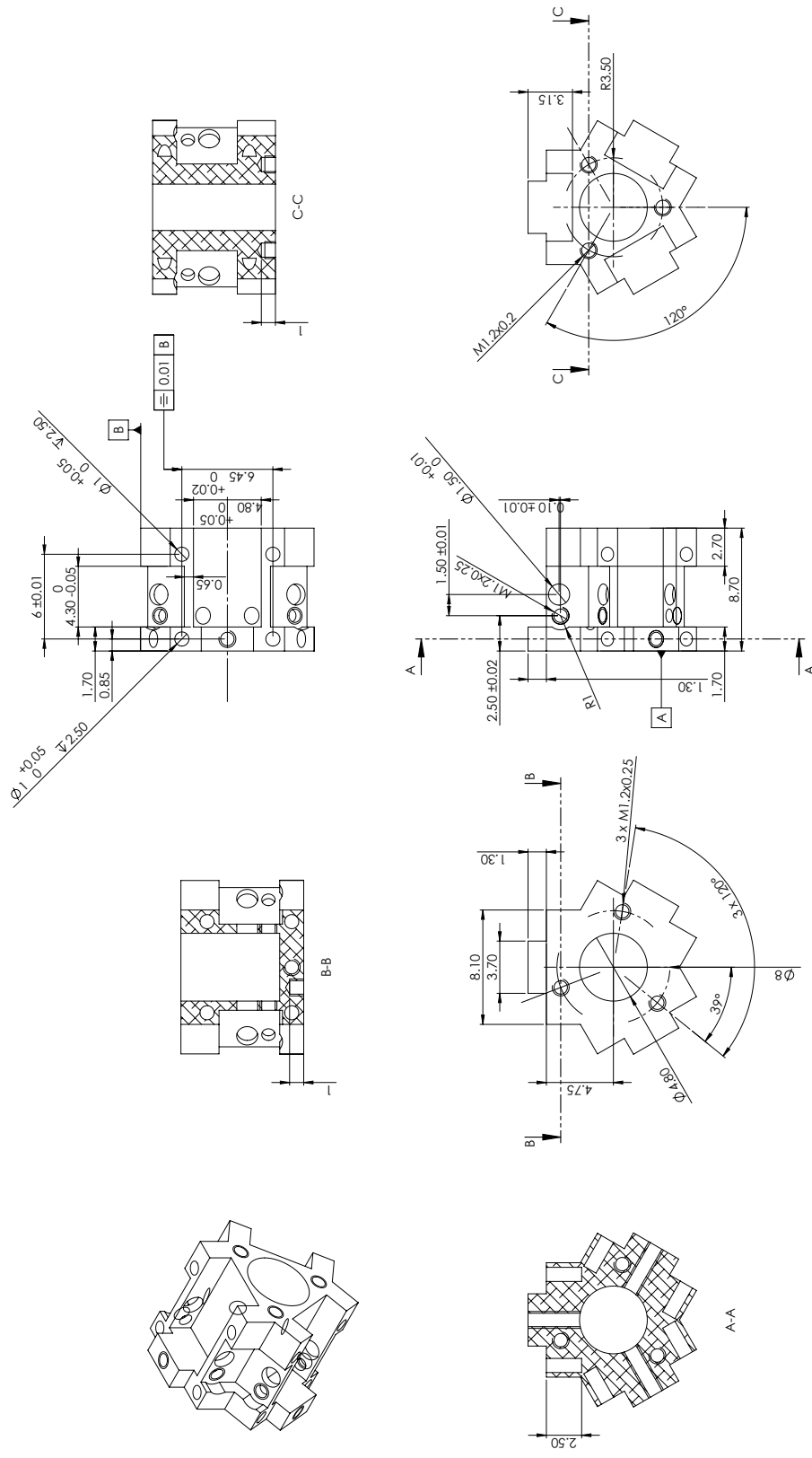


Figure B.3. Technical drawing of 3-DOF PRD's main base. All dimensions are in mm.

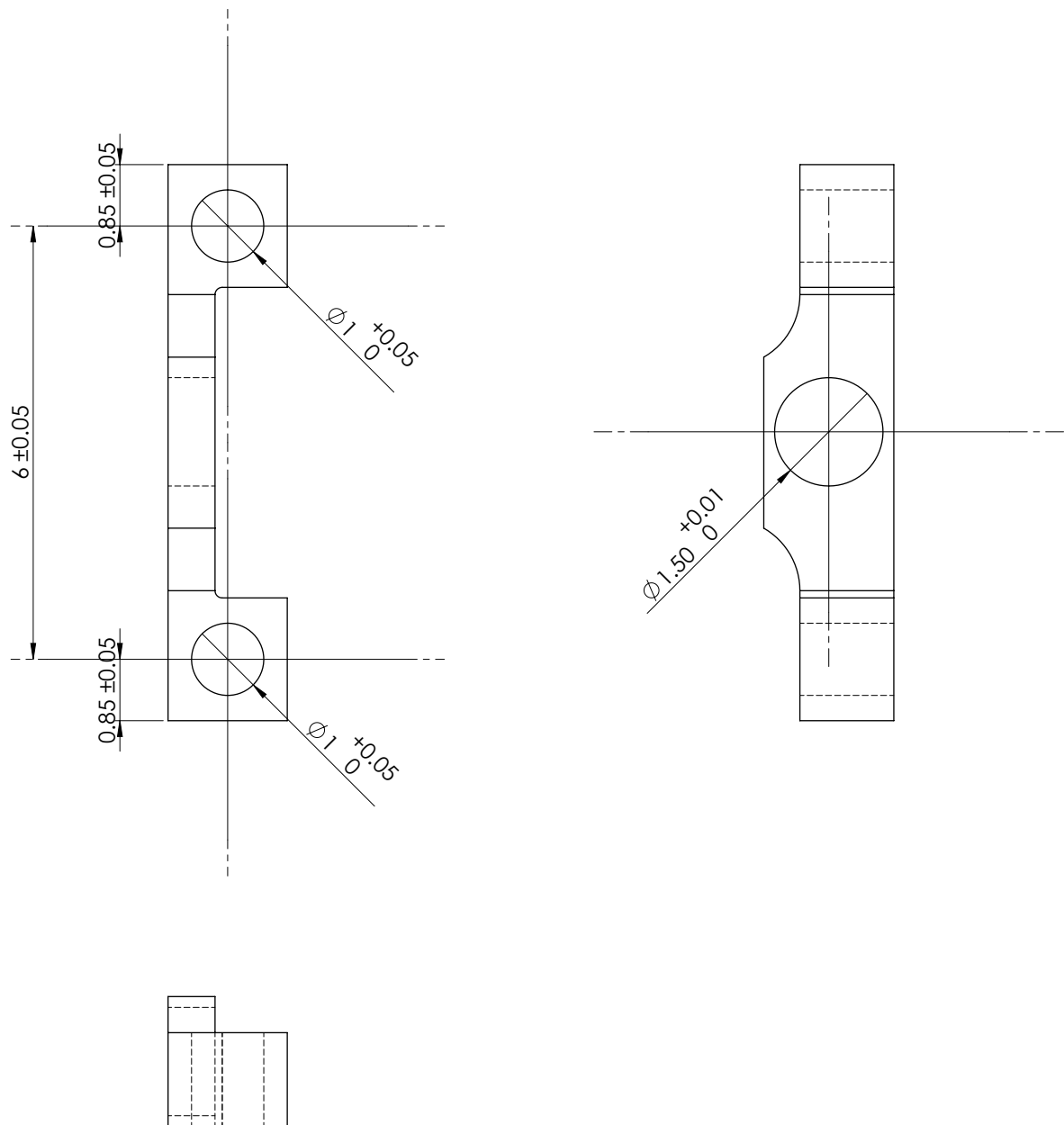


Figure B.4. Technical drawing of 3-DOF PRD's moving base. All dimensions are in mm.

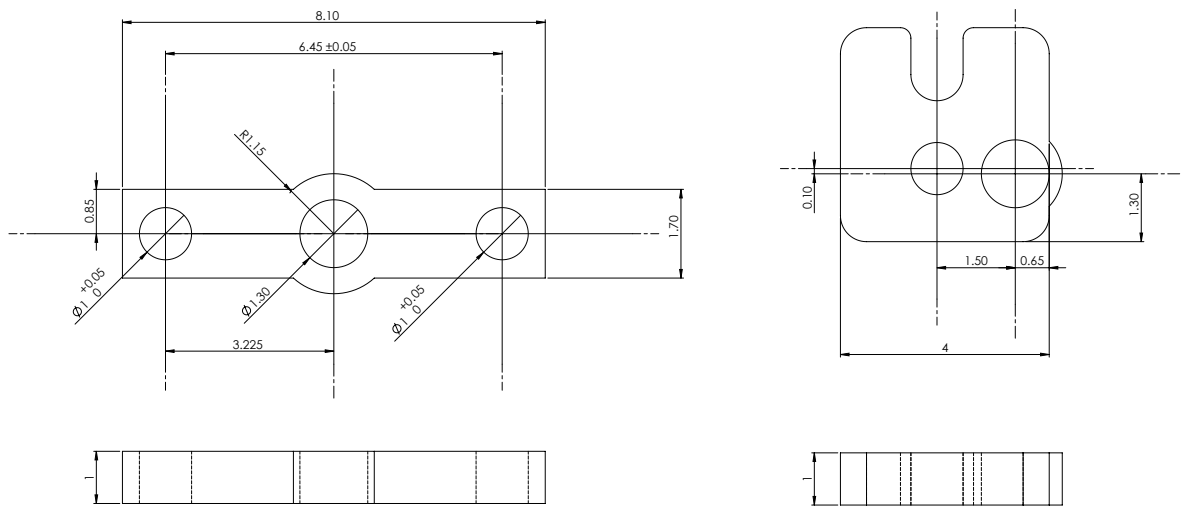


Figure B.5. Technical drawings of 3-DOF PRD's roller adjustment plate (left) and bearing cover (right). All dimensions are in mm.

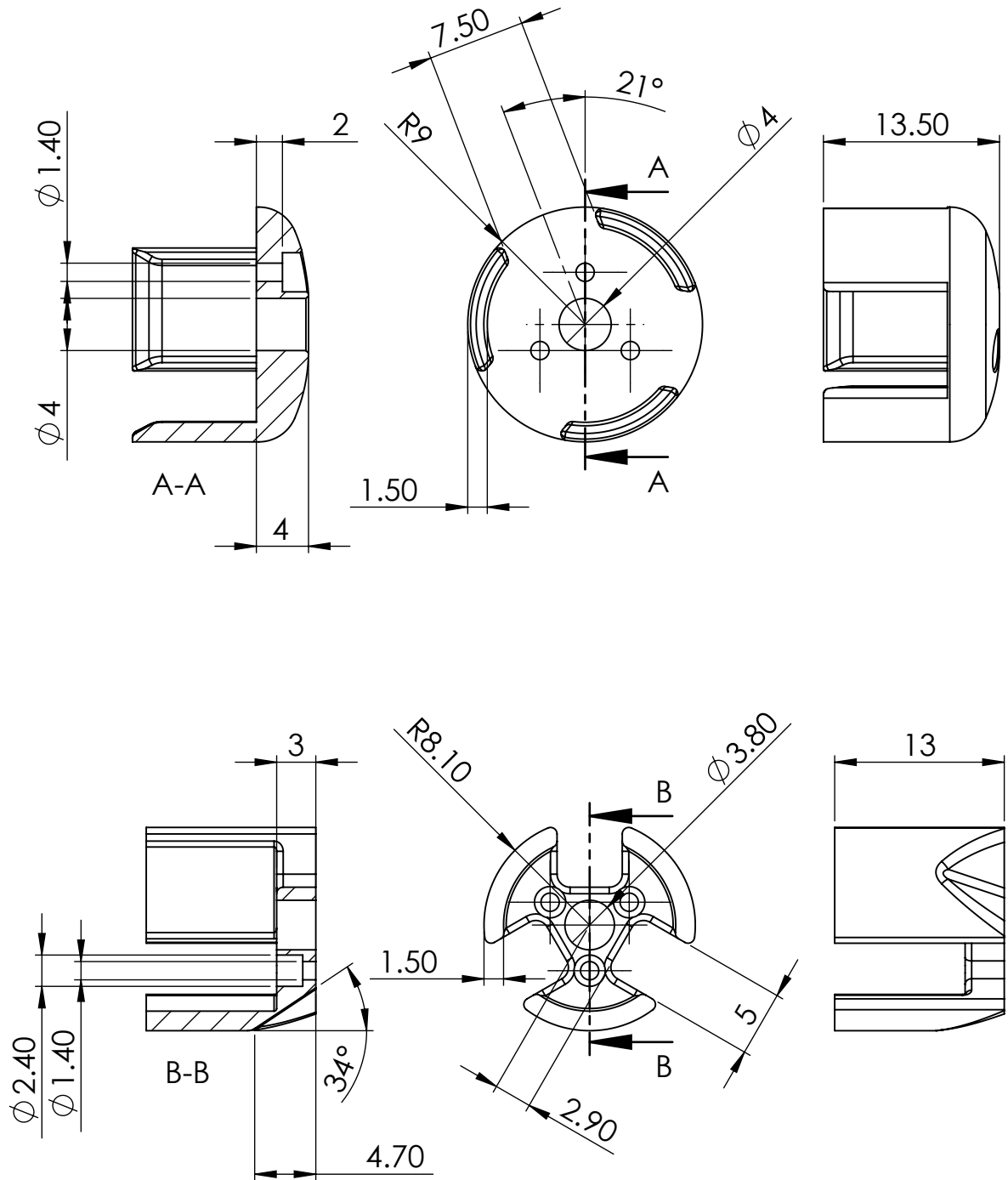


Figure B.6. Technical drawings of sheath retainer (top) and shell retainer (bottom) at tip. All dimensions are in mm.

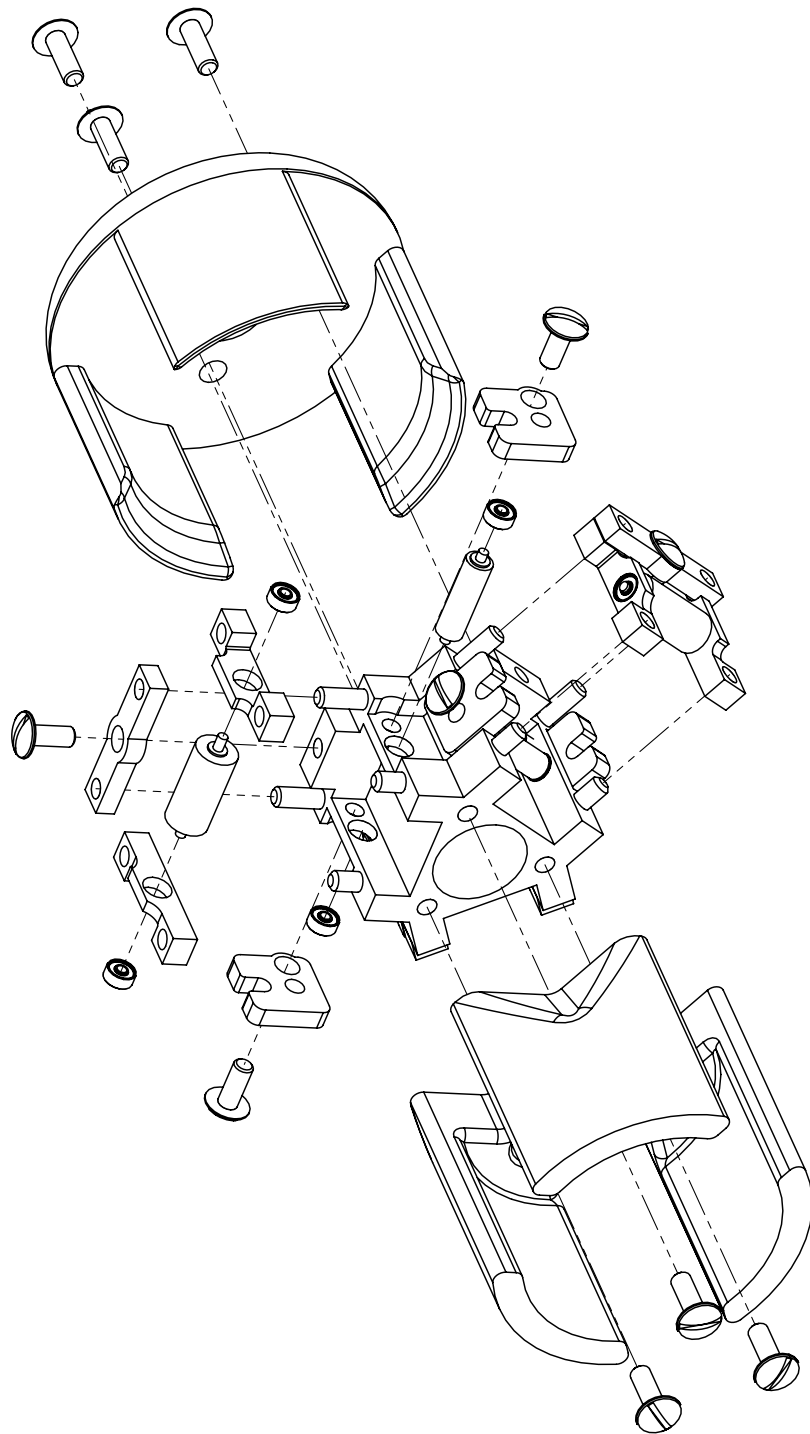


Figure B.7. Technical drawing showing 3-DOF PRD's assembly.

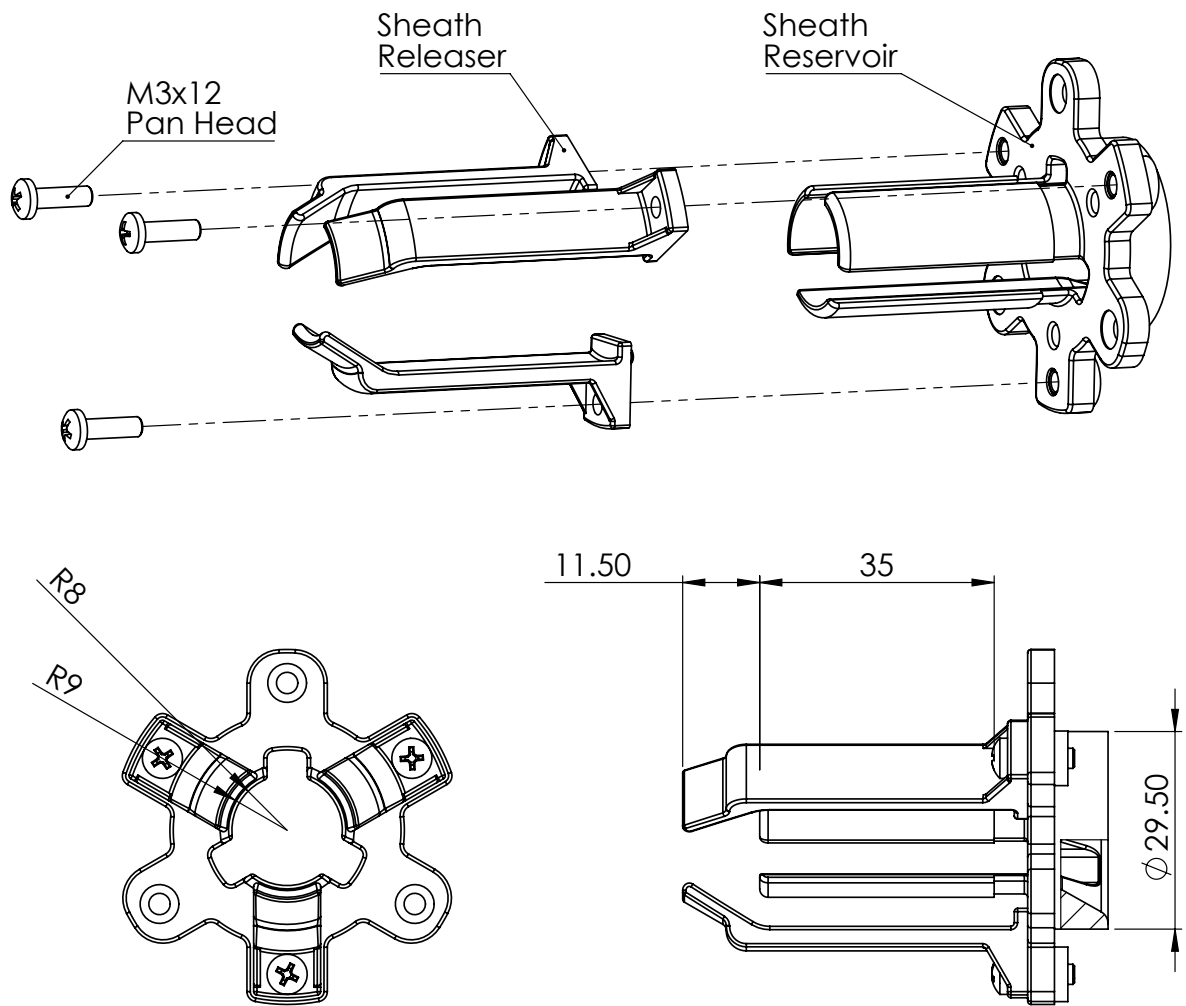


Figure B.8. Technical drawing of sheath feed mechanism. All dimensions are in mm.

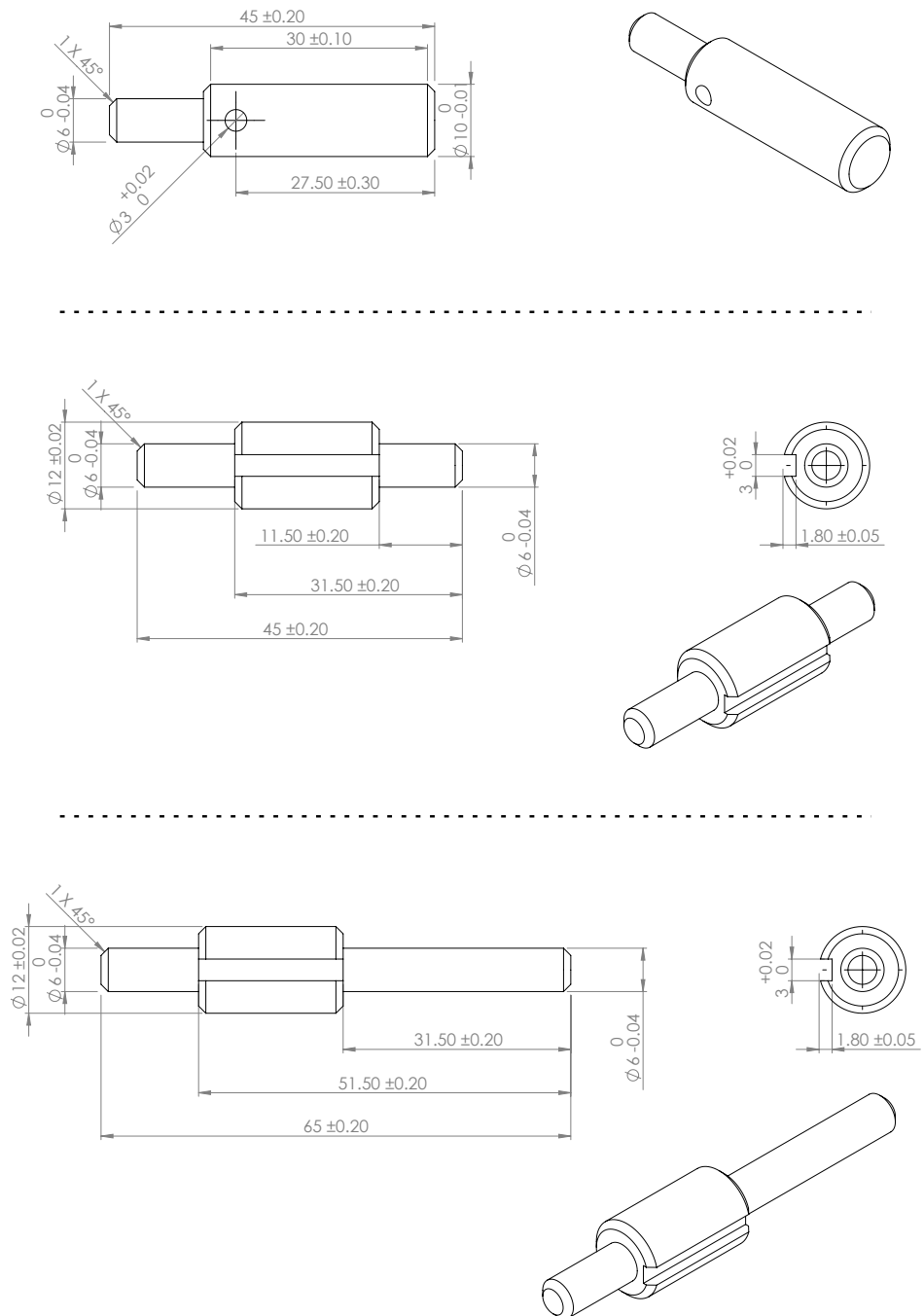


Figure B.9. Technical drawings of worm shaft (top) and worm gear shafts (middle and bottom) used in tubing feed mechanism. All dimensions are in mm.

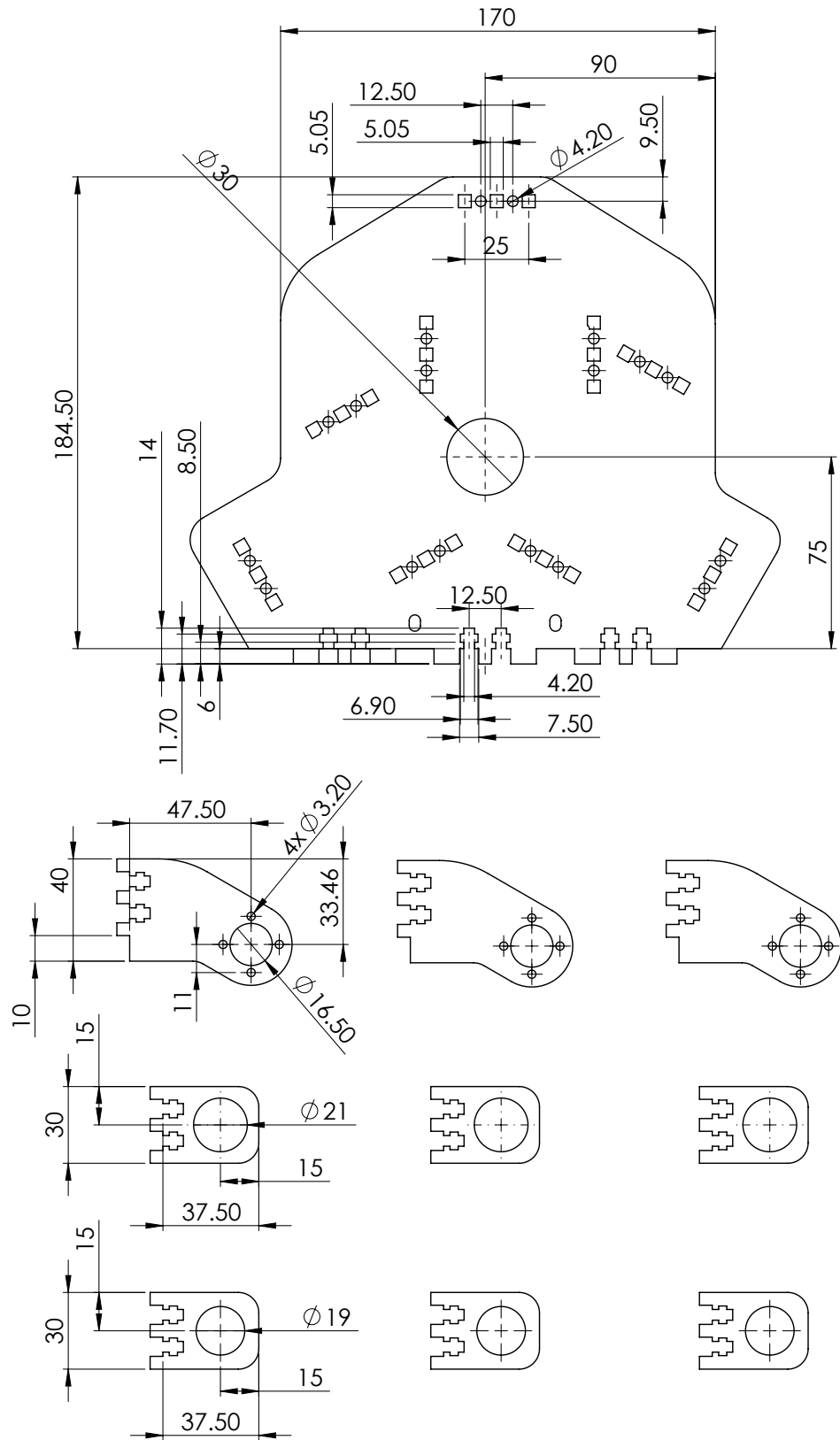


Figure B.10. Technical drawings of base sheets of tubing feed mechanism. Thickness is 5 mm. All dimensions are in mm.

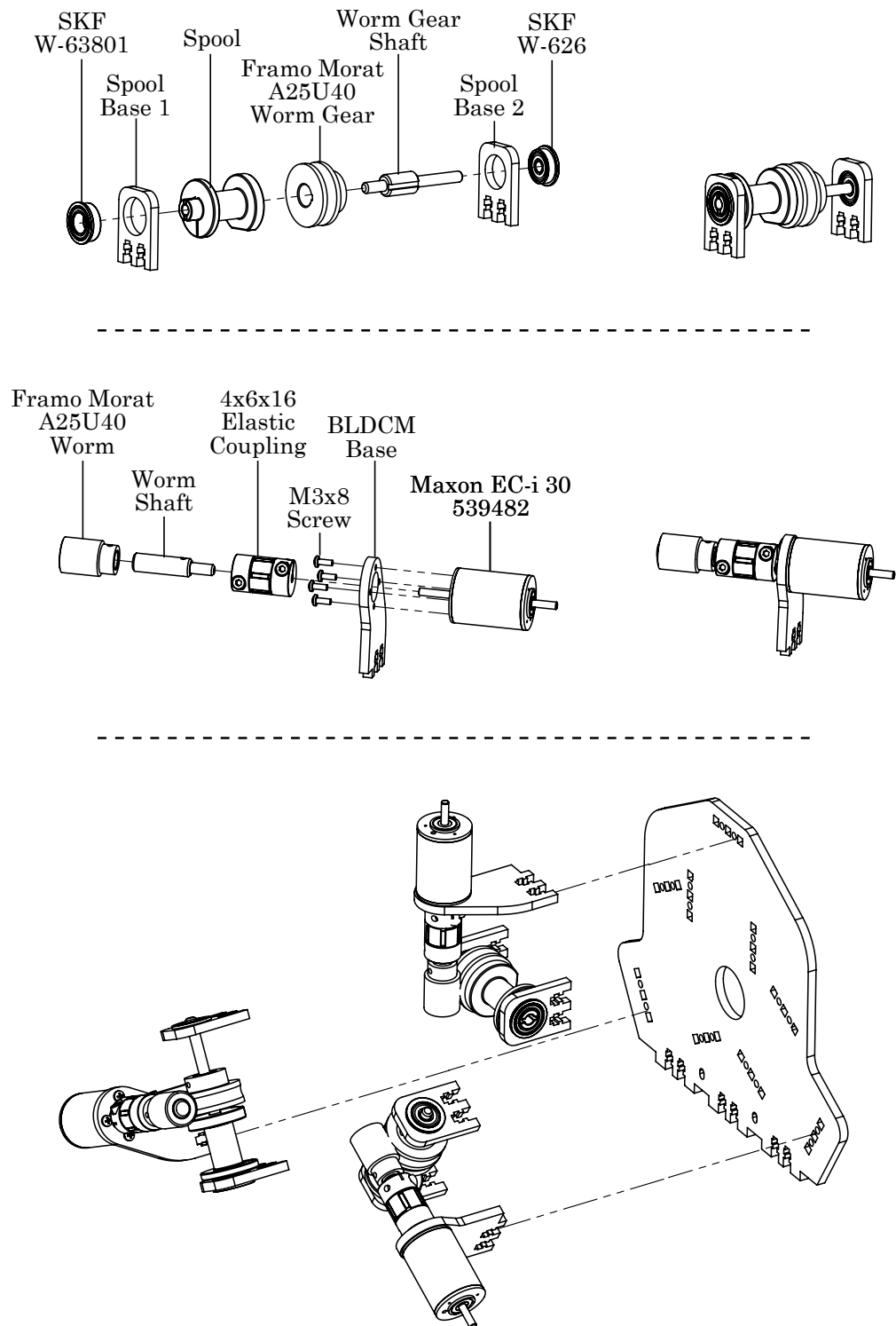


Figure B.11. Technical drawings showing worm gear (top) and worm (middle) sub-assemblies and overall (bottom) assembly of tubing feed mechanism.